Supporting information

Performance of SIFT-MS and PTR-MS in the measurement of volatile organic compounds at different humidities

Ann-Sophie Lehnert[1,2], Thomas Behrendt[1], Alexander Ruecker[1], Georg Pohnert[2], Susan Trumbore[1]

[1]Max Planck Institute for Biogeochemistry, 07745 Jena, Germany
[2]Institute for Inorganic and Analytical Chemistry, Friedrich Schiller University, 07743 Jena, Germany

Correspondence to: Ann-Sophie Lehnert (alehnert@bgc-jena.mpg.de)

Number of pages: 28

Number of figures: 23

Number of tables: 11

S1 SIFT-MS optimization to reduce background

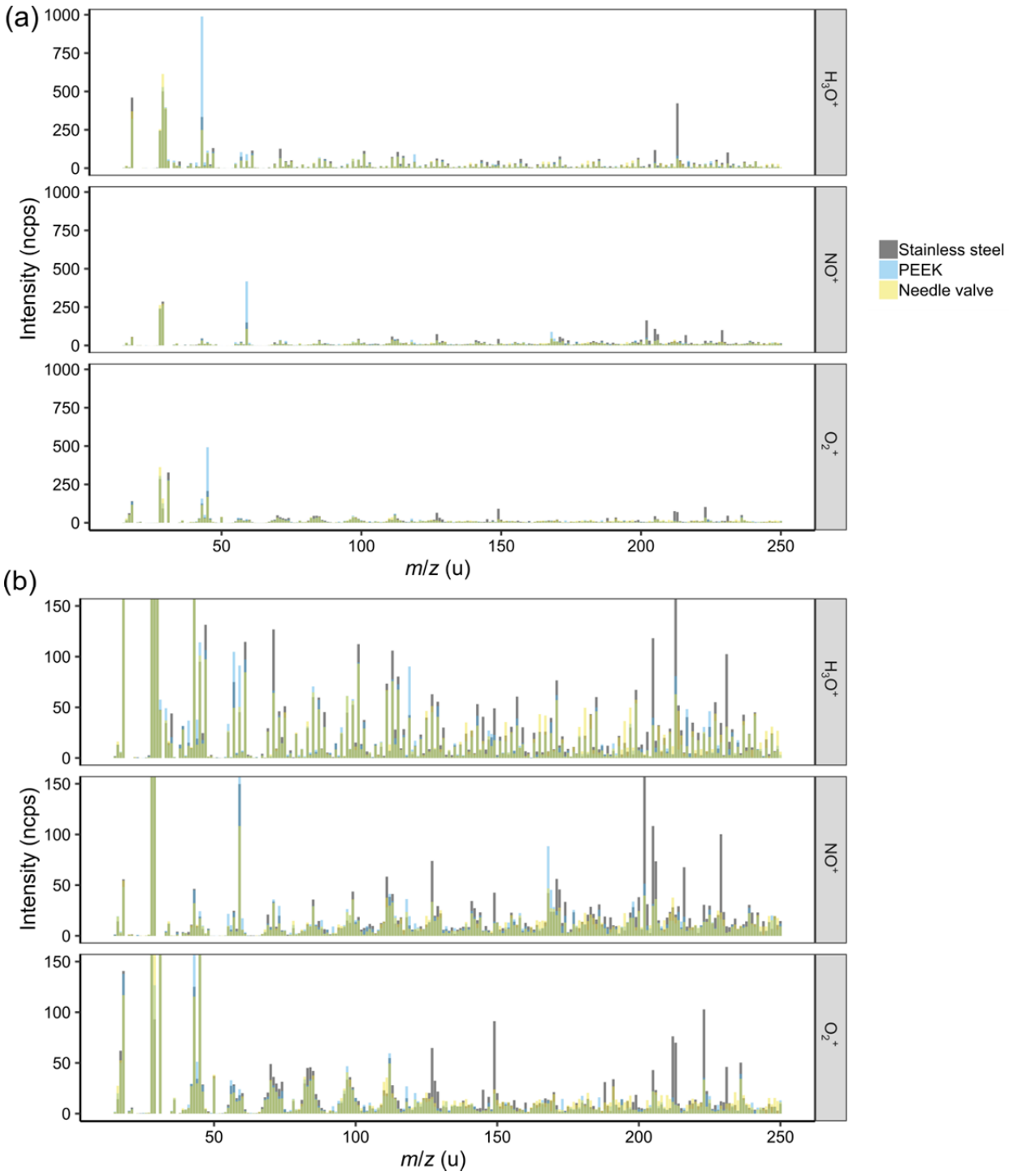

Figure S1: Background as recorded for different flow restrictors in the multi-port inlet: capillaries from silica coated stainless steel (as provided by Syft Technologies, grey bars), from PEEK (blue bars), and a Swagelok needle valve (yellow bars). The ion intensity is normalized to 10^6 counts of the reagent ion and the air flow entering the system in sccm. (b) is a zoomed-in version of (a), to visualize differences better. The reagent ions as well as their water clusters and isotopic peaks are not shown to improve clarity.

We chose to use the needle valve since it consistently shows lowest contamination in the range <150 u.

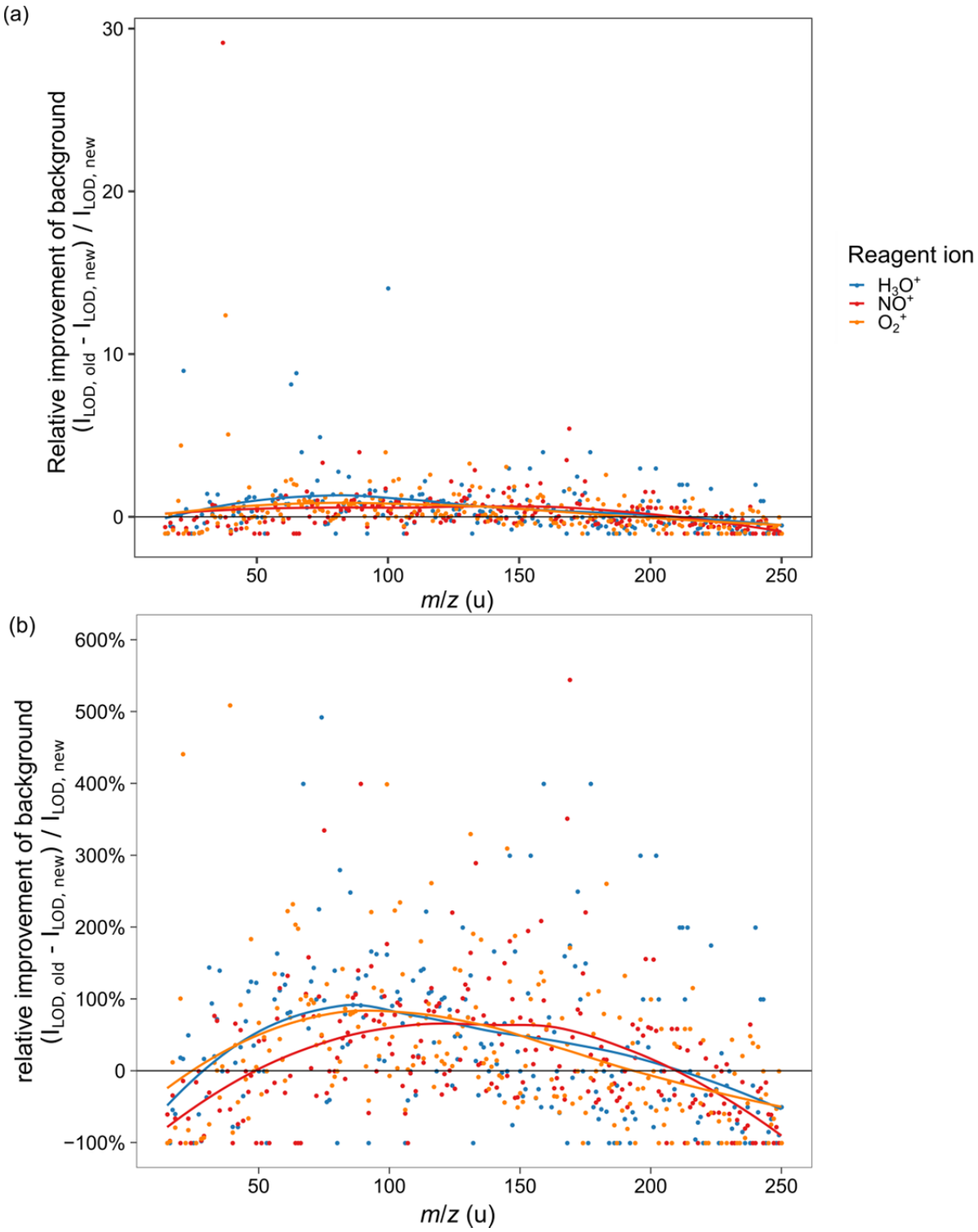

Figure S2: Relative improvement of the instrument background (instrument being flushed with VOC free air) after changing the o-rings in the system to FEP coated FKM o-rings. Comparing the critical intensity $\boldsymbol{I_{LOD} = \overline{I_{background}} + 3 \cdot sd(I_{background})}$ before (old) and after (new) the change, normalized to the critical intensity after the o-ring change. (a) complete display of all improvement factors, (b) zoomed plot for lower relative improvements. The data was normalized to 10^6 reagent ion counts before comparing it. Changes in secondary reagent ions, i.e. H_3O^+ / 30, 32, 37, 55, 73, NO^+ / 19, 32, 37, 48, O_2^+ / 19, 30, 37 as well as reagent ion isotopic peaks were removed from the data before plotting. The curves are LOESS fits of the critical intensities with regard to the three reagent ions.

We found H_3O^+ 63, 65, 67, and 114 u and O_2^+ 63, and 64, which might all be different ions of difluorovinylidene quenching products and residual monomers, $[CF_2CH]^+$, $[CF_2CH_3]^+$, $[CF_2CH_5]^+$, $[C_2F_4CH_2]^+$, and $[CF_2CH_2]^+$. H_3O^+ 100 u might be $[C_2F_4]^+$, 202 u might be $[C_4F_8H_2]^+$, 196 and 146 u could be $[HC_2F_4CO_2H]^+$ and $[HCF_2CO_2H]^+$, NO^+ 169 could be $[C_3F_7]^+$, and O_2^+ 102 amu could be $[C_2F_4H_2]^+$ which might be byproducts in the PTFE production or degradation. This all hints to the fact that the previous o-rings in the system degassed small contaminants that could come from their production process.

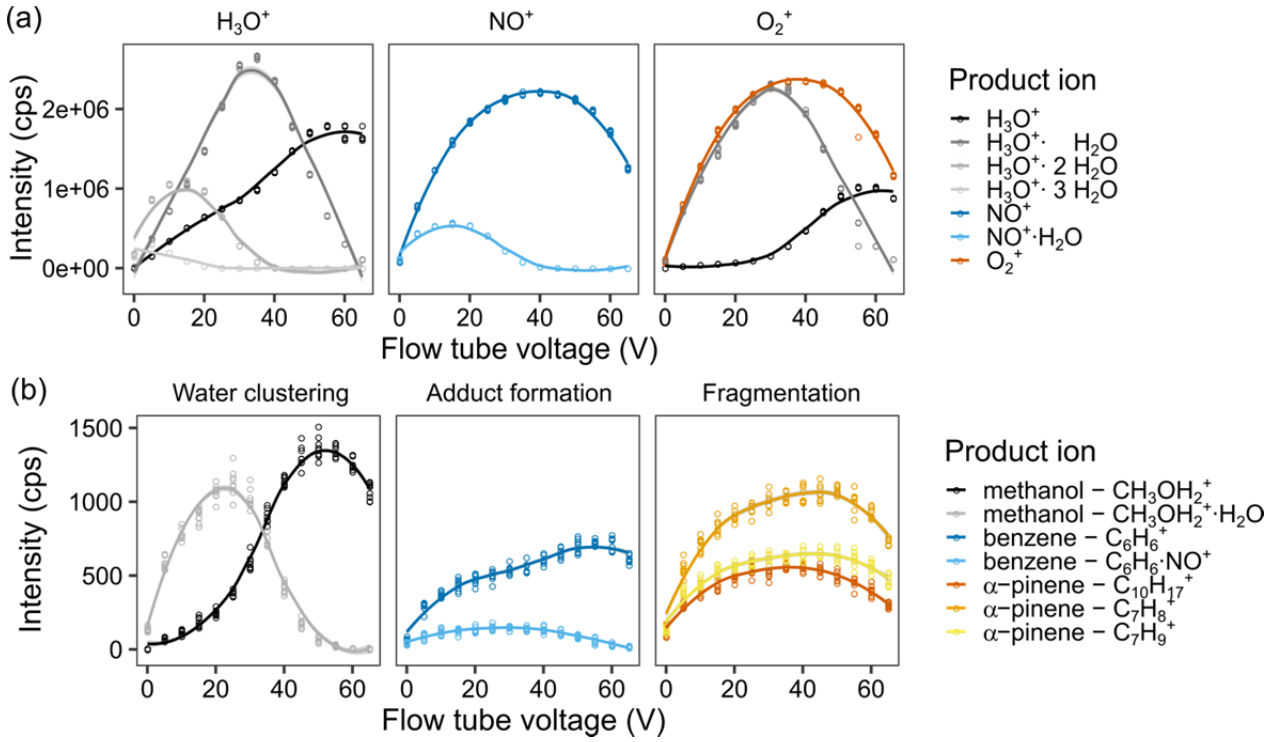

Figure S3: Effect of the flow tube voltage on reagent and product ion counts. (a) intensity of the different measured product ions when selecting for H_3O^+ (left), NO^+ (middle) and O_2^+ (right) in the first quadrupole. (b) examples of the product ion behaviour illustrating the effect of water clustering on the methanol ions reacting with H_3O^+ (left), adduct formation on the benzene ions upon reaction with NO^+ (middle), and fragmentation of the α-pinene ions upon reaction with O_2^+ (right). Measurements were done for a humid (90% at 25°C) 5 ppb VOC standard air flow, and were fit *via* LOESS. For the results of all ions, cf. Fig. S9.

With higher flow tube voltage, *i.e.* a higher kinetic energy of the ions, we expected (i) a higher reaction efficiency in general, leading to more ions, (ii) more secondary reagent ions, e.g. more H_3O^+ when O_2^+ was the reagent ion, (iii) less water clustering, (iv) less adduct formation and (v) more fragmentation. In (b), one can see that (iii) and (iv) are definitely true, (v) does occur a bit, but hardly at all, and (i) and (ii) did not occur the way we expected it. For (i), we assume that this is due to the fact that a third particle is needed in order to take up excess kinetic energy. If the kinetic energy is too high, the collisional cross section is too small and the partner cannot take up the excess, and the reaction partners move away from each other again, as described by Smith and Spanel, 2005. Interestingly, overall reagent ion counts of NO^+ and O_2^+ decrease with a higher flow tube voltage, but the other ion counts do not increase in the same manner. We are unsure what causes this since we expected to see an increased signal by increased focusing of the ions. Maybe, they are hitting one of the accelerating electrode instead of being focused by the lenses. So as a compromise between fighting water clustering and loosing NO^+ and O_2^+ reagent ions, 40 V were chosen as a flow tube voltage.

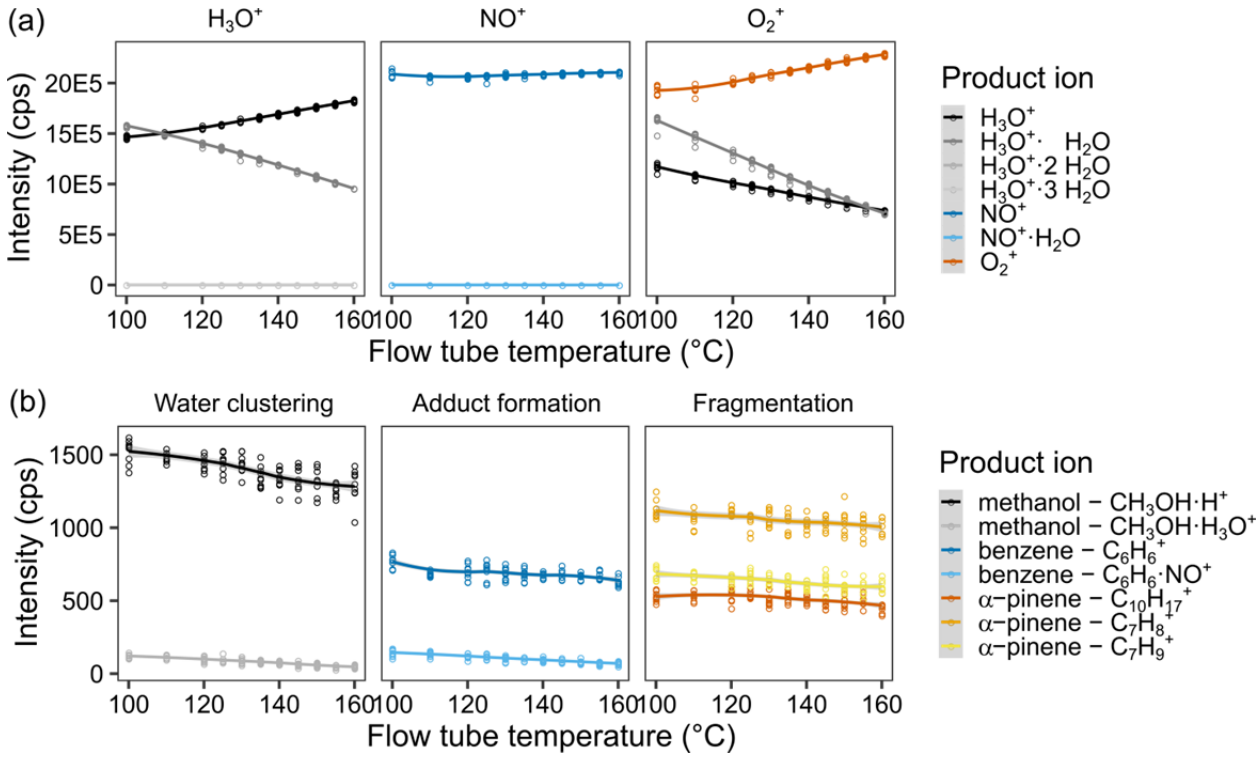

Figure S4: Effect of the flow tube temperature on reagent and product ion counts. (a) intensity of the different measured product ions when selecting for H_3O^+ (left), NO^+ (middle) and O_2^+ (right) in the first quadrupole. (b) examples of the product ion behaviour illustrating the effect of water clustering on the methanol ions reacting with H_3O^+(left), adduct formation on the benzene ions upon reaction with NO^+(middle), and fragmentation of the α-pinene ions upon reaction with O_2^+(right). Measurements were done for a humid (90% @ 25°C) 5 ppb VOC standard air flow, and were fit *via* LOESS. For results of all measured ions, cf. Fig. S8.

Increasing the flow tube temperature also increases the kinetic energy, but randomly and of all molecules inside the flow tube, not just the ions. The same effects were expected as for the flow tube voltage, but in comparison to that, the effects are rather small. One can see a slight decrease in product ion counts, cf. Figure S3. Only for the reagent ion counts, one can see a major shift decreasing interfering ions, thus, a flow tube temperature as high as possible appears to be advantageous. However, the authors were concerned that for environmental samples, the thermal stability of some gases might be smaller so that the more labile compounds might not be detected. Thus, we decided on a flow tube temperature of 140°C.

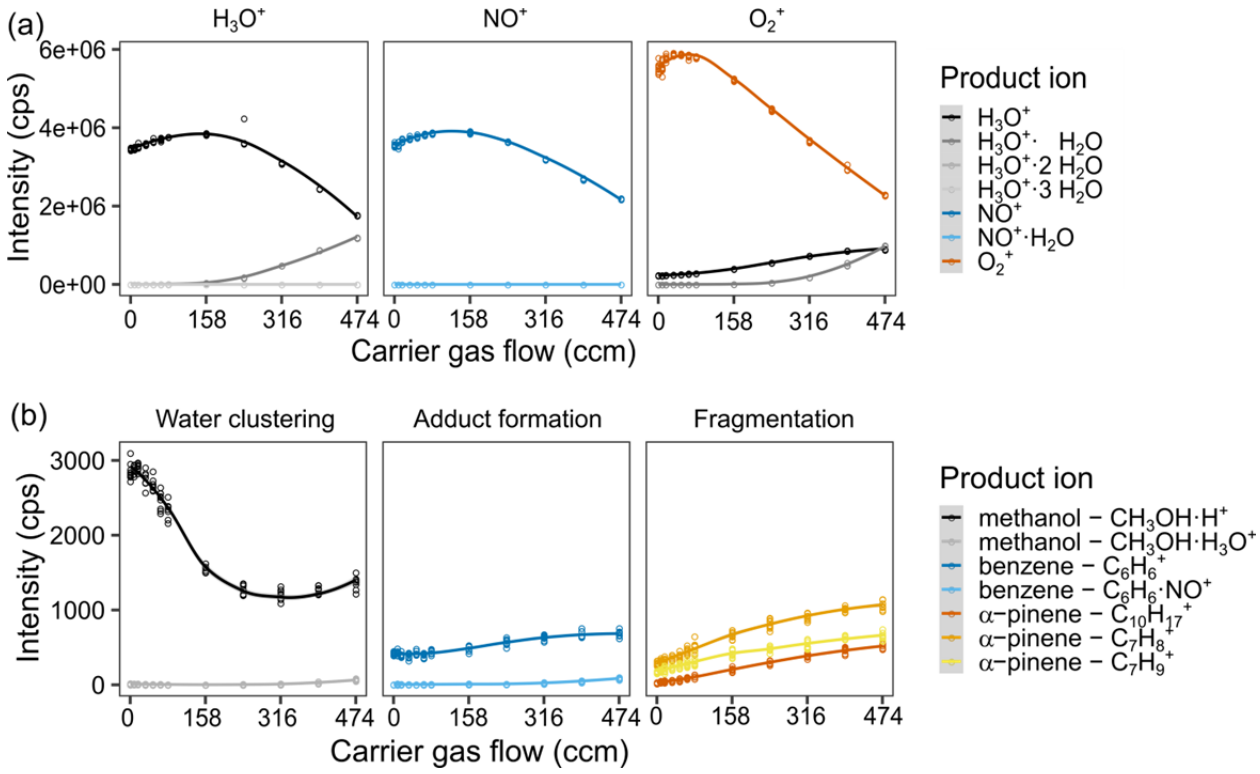

Figure S5: Effect of the helium carrier gas flow on reagent and product ion counts. (a) intensity of the different measured product ions when selecting for H_3O^+ (left), NO^+ (middle) and O_2^+ (right) in the first quadrupole. (b) examples of the product ion behaviour illustrating the effect of water clustering on the methanol ions reacting with H_3O^+ (left), adduct formation on the benzene ions upon reaction with NO^+ (middle), and fragmentation of the α-pinene ions upon reaction with O_2^+. Measurements were done for a humid (90% @ 25°C) 5 ppb VOC standard air flow, and were fit *via* LOESS. The sample gas flow was 120 sccm (capillary with 0.010" inner diameter). For complete results of all measured ions, cf. Fig. S7.

Increasing the carrier gas flow while keeping the sample gas flow stable meant increasing the pressure in the flow tube. This both decreases the main free path of the ions and provides more collision partners. Thus, on the one hand, reactions are expected to be more efficient since surplus energy can be dissipated easier into the system, but on the other hand, ions are expected to be colder on average since the energy is dissipated stronger in the system. Diffusion to the walls should be decreased by that. For clustering and adduct formation, both effects come into play – the reaction forming those clusters should be more effective, but also the reaction taking them apart. Reagent ion counts are highest at low amounts of carrier gas, and product ion counts are increasing with increasing pressure, since the reaction is getting more efficient. At low carrier gas flows, the diffusion to the walls is most efficient, leading to an optimum point for the reagent ion counts. The decrease in their intensity for higher carrier gas flows should be due to more reactions. Water clustering, adduct formation, and fragmentation are not changing significantly when changing the carrier gas flow. Methanol is an interesting example though, since its counts are highest for low carrier gas flows. What causes this is unclear since it is counteracting the trends of the other product ions, but might be due to a contamination in the system, as a similar effect is observed for sample gas flows, *cf*. Figure S6. For a carrier gas flow, 4 $TorrLs^{-1}$ were chosen to ensure high product ion counts whilst not losing too much reagent ion intensity.

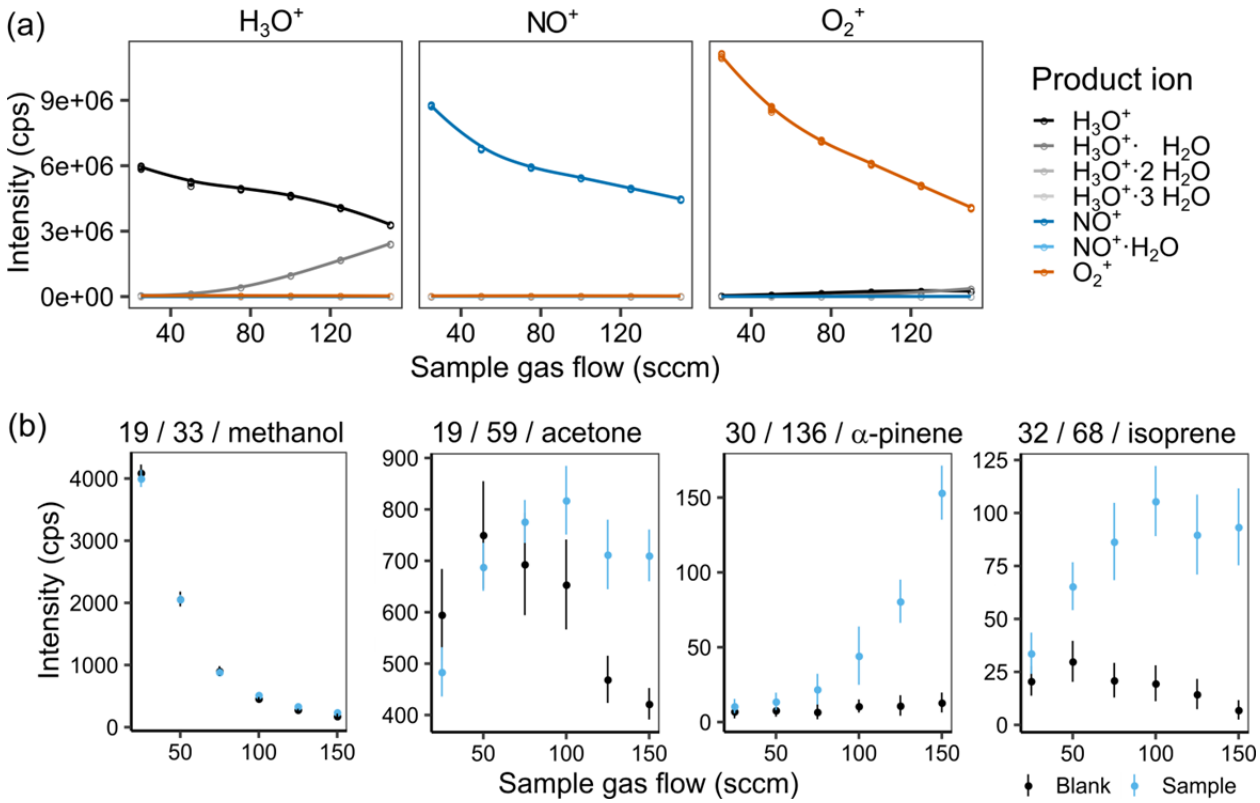

Figure S6: Effect of the sample gas flow on the intensity of the different measured product ions when selecting for H_3O^+ (left), NO^+ (middle) and O_2^+ (right) in the first quadrupole (a) and the product ion intensity for a Zero Air blank and a 1ppb VOC standard sample for methanol, acetone, α-pinene and isoprene at 60% humidity (25°C) (b). In (b), the captions are labelled with *m/z* of the reagent ion, *m/z* of the product ion, and the corresponding substance. The helium carrier gas flow was kept at 158 sccm (2 TorrL s^{-1}).

As was expected, the product ions increase with increasing sample gas flow in most cases, and also water clustering increases. However, we were surprised to see that the effect of water clustering was not critical for the chosen settings: the amount of unreactive m/z = 55 u was negligible, and no H_3O^+ signals were visible in the other two reagent ion channels. However, this experiment was done at a medium humidity, so to be save, a sample gas flow of 125 sccm was chosen.

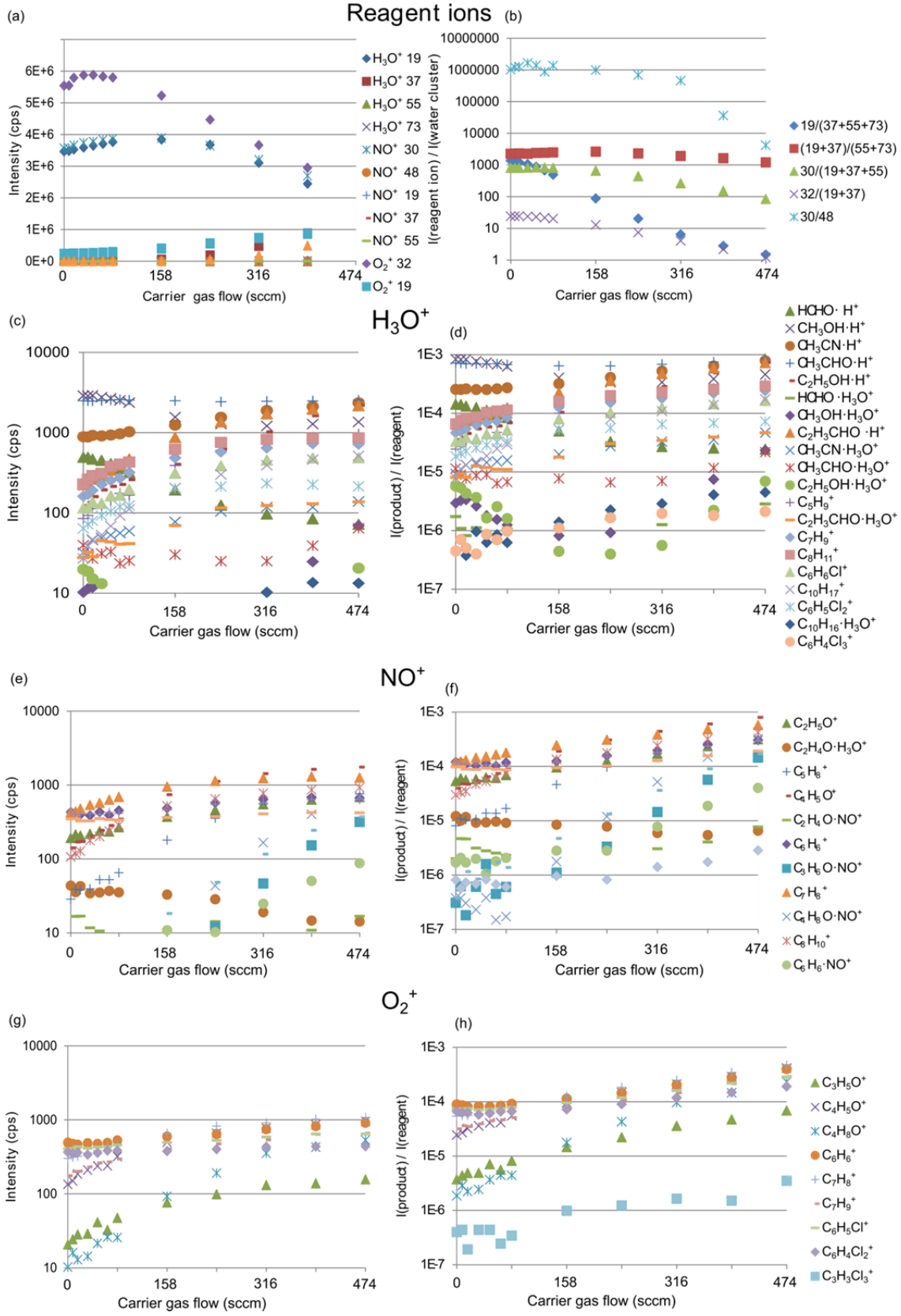

Figure S7: Complete results of the carrier gas flow optimization for helium carrier gas and zero air dilution gas, U_{FT} = 50 V, T_{FT} = 140°C, 90% humidity at 25°C. (a), (b): for the different reagent ions H_3O^+, NO^+, and O_2^+, the detected primary and secondary reagent ions symbolized by their mass are shown 19 = H_2O^+, 37 = $H_3O^+ \cdot H_2O$, 55 = $H_3O^+ \cdot 2\ H_2O$, 73 = $H_3O^+ \cdot 3\ H_2O$, 30 = NO^+, 48 = $NO^+ \cdot H_2O$, 32 = O_2^+. (a): absolute ion counts, (b): proportion of reagent ions relative to the water clusters. (c–h): behaviour of the product ions upon reaction with H_3O^+ (19 + 37 + 55, (c, d)), NO^+ (e, f), and O_2^+ (g, h) as reagent ions. (c, e, g): absolute ion counts, (d, f, h): counts normalized to reagent ion counts.

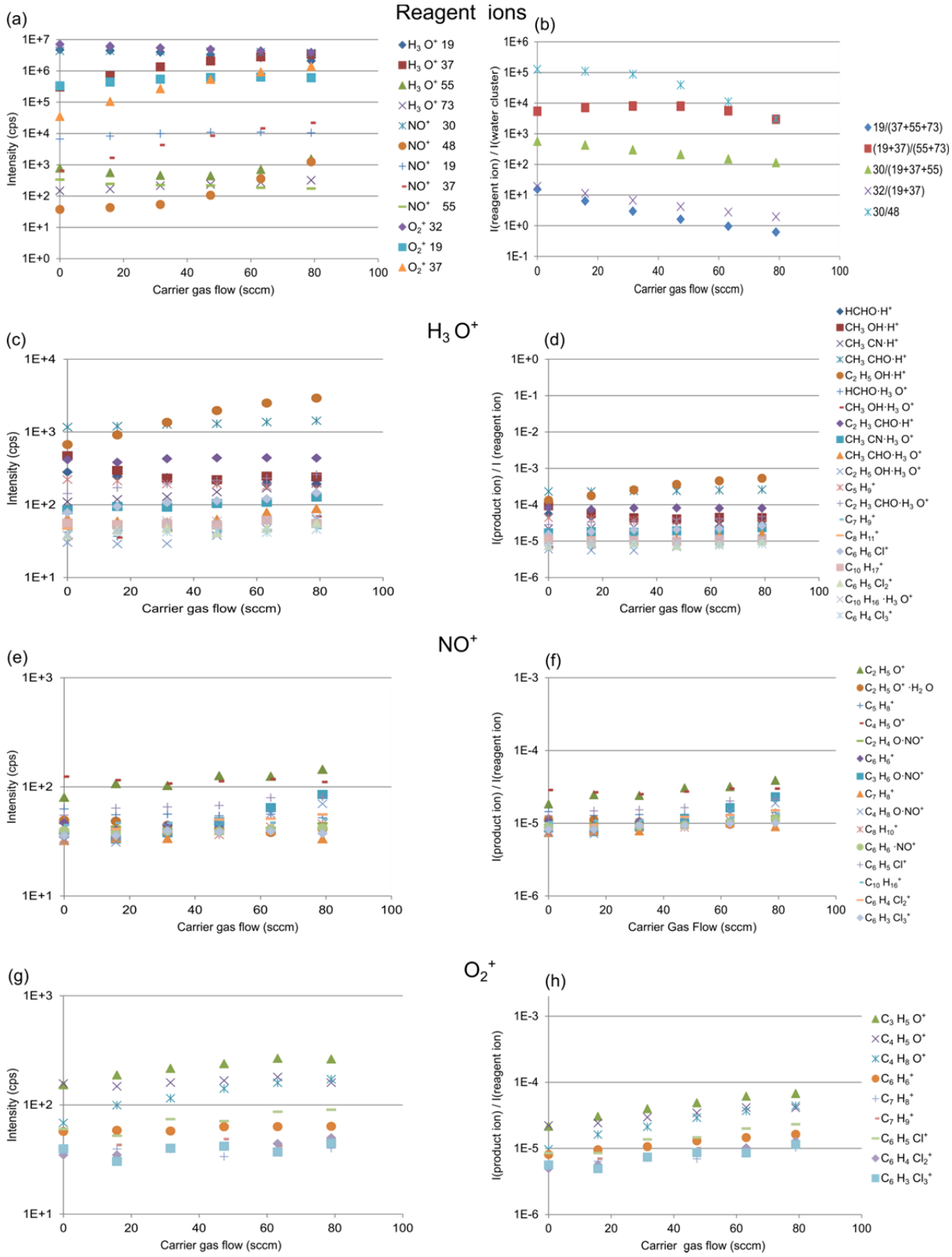

Figure S8: Complete results of the carrier gas flow optimization for helium carrier gas and zero air dilution gas, U_{FT} = 50 V, T_{FT} = 140°C, 90% humidity at 25°C, picture section of Fig. S7 for low carrier gas flows <100 sccm. (a), (b): for the different reagent ions H_3O^+, NO^+, and O_2^+, the detected primary and secondary reagent ions symbolized by their mass are shown 19 = H_2O^+, 37 = $H_3O^+ \cdot H_2O$, 55 = $H_3O^+ \cdot 2\ H_2O$, 73 = $H_3O^+ \cdot 3\ H_2O$, 30 = NO^+, 48 = $NO^+ \cdot H_2O$, 32 = O_2^+. (a): absolute ion counts, (b): proportion of reagent ions relative to the water clusters. (c–h): behaviour of the product ions upon reaction with H_3O^+ (19 + 37 + 55, (c, d)), NO^+ (e, f), and O_2^+ (g, h) as reagent ions. (c, e, g): absolute ion counts, (d, f, h): counts normalized to reagent ion counts.

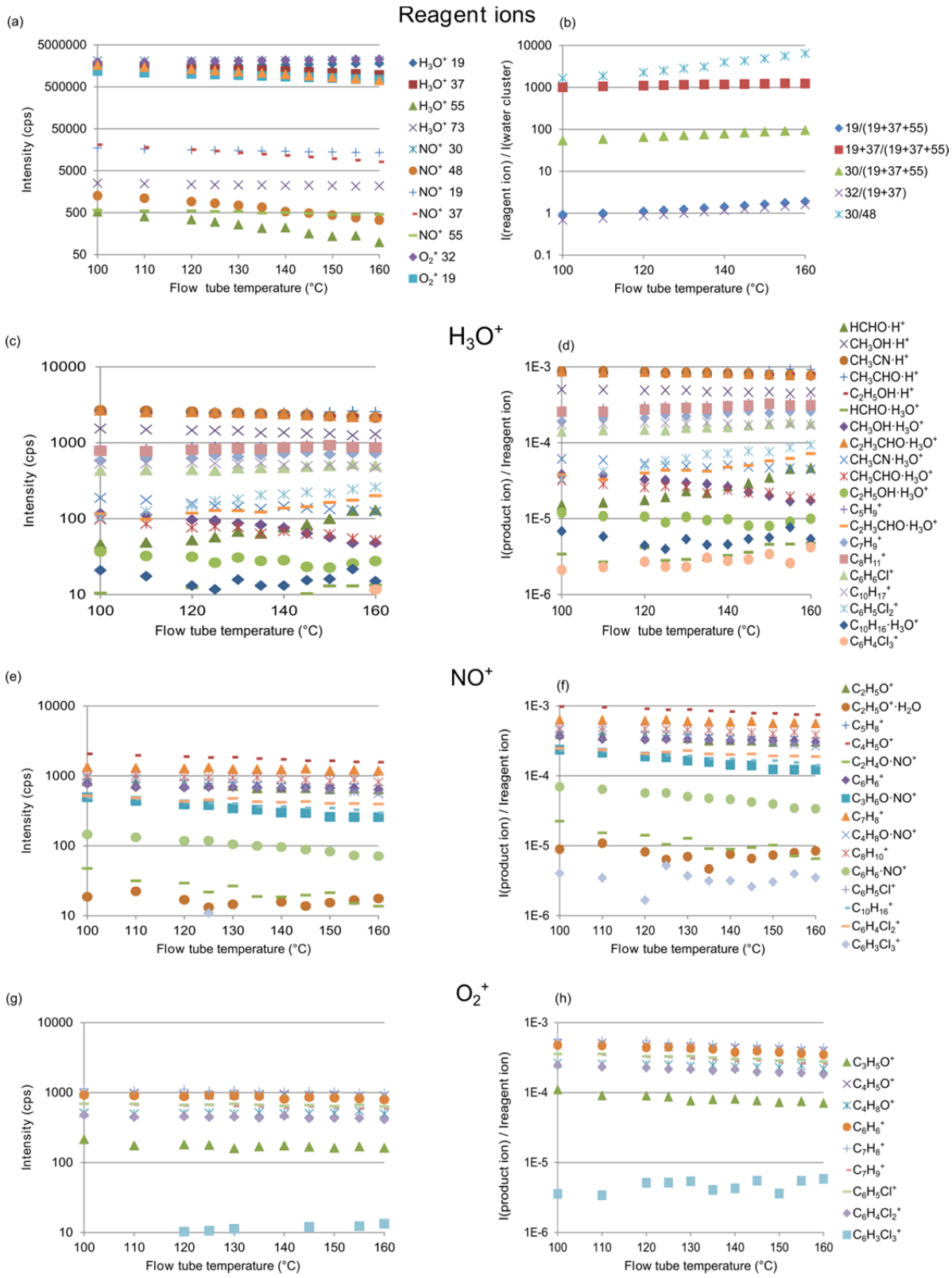

Figure S9: Complete results of the flow tube temperature for helium carrier gas and zero air dilution gas, U_{FT} = 50 V, ϕ_{FT} = 395 sccm, 90% humidity at 25°C.(a–b) for the different reagent ions H_3O^+, NO^+, and O_2^+, the detected primary and secondary reagent ions symbolized by their mass are shown 19 = H_2O^+, 37 = $H_3O^+ \cdot H_2O$, 55 = $H_3O^+ \cdot 2\ H_2O$, 73 = $H_3O^+ \cdot 3\ H_2O$, 30 = NO^+, 48 = $NO^+ \cdot H_2O$, 32 = O_2^+. (a) absolute ion counts, (b) proportion of reagent ions relative to the water clusters. (c–h) behaviour of the product ions upon reaction wih H_3O^+ (19 + 37 + 55, c, d), NO^+ (e, f), and O_2^+ (g, h) as reagent ions. (c, e, g) absolute ion counts, (d, f, h) counts normalized to reagent ion counts.

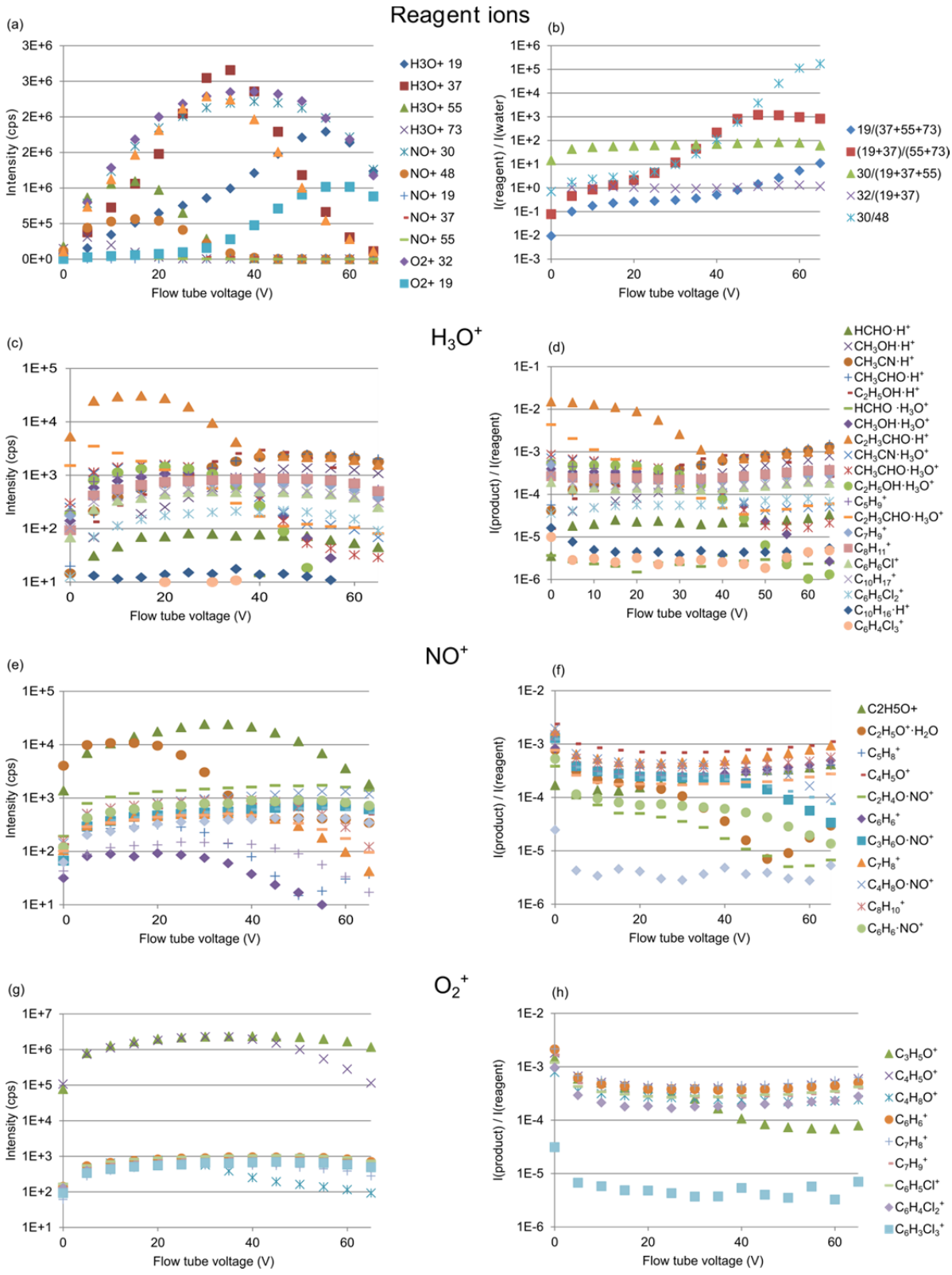

Figure S10: Flow tube voltage optimization for helium carrier gas and zero air dilution gas, ϕ_{FT} = 395 sccm, T_{FT} = 140°C, 90% humidity at 25°C. (a–b) for the different reagent ions H_3O^+, NO^+, and O_2^+, the detected primary and secondary reagent ions symbolized by their massare shown 19 = H_2O^+, 37 = $H_3O^+ \cdot H_2O$, 55 = $H_3O^+ \cdot 2\ H_2O$, 73 = $H_3O^+ \cdot 3\ H_2O$, 30 = NO^+, 48 = $NO^+ \cdot H_2O$, 32 = O_2^+. (a) absolute ion counts, (b) proportion of reagent ions relative to the water clusters. (c–h) behaviour of the product ions upon reaction with H_3O^+ (19 + 37 + 55, c, d), NO^+ (e, f), and O_2^+ (g, h) as reagent ions. (c, e, g) absolute ion counts, (d, f, h) counts normalized to reagent ion counts.

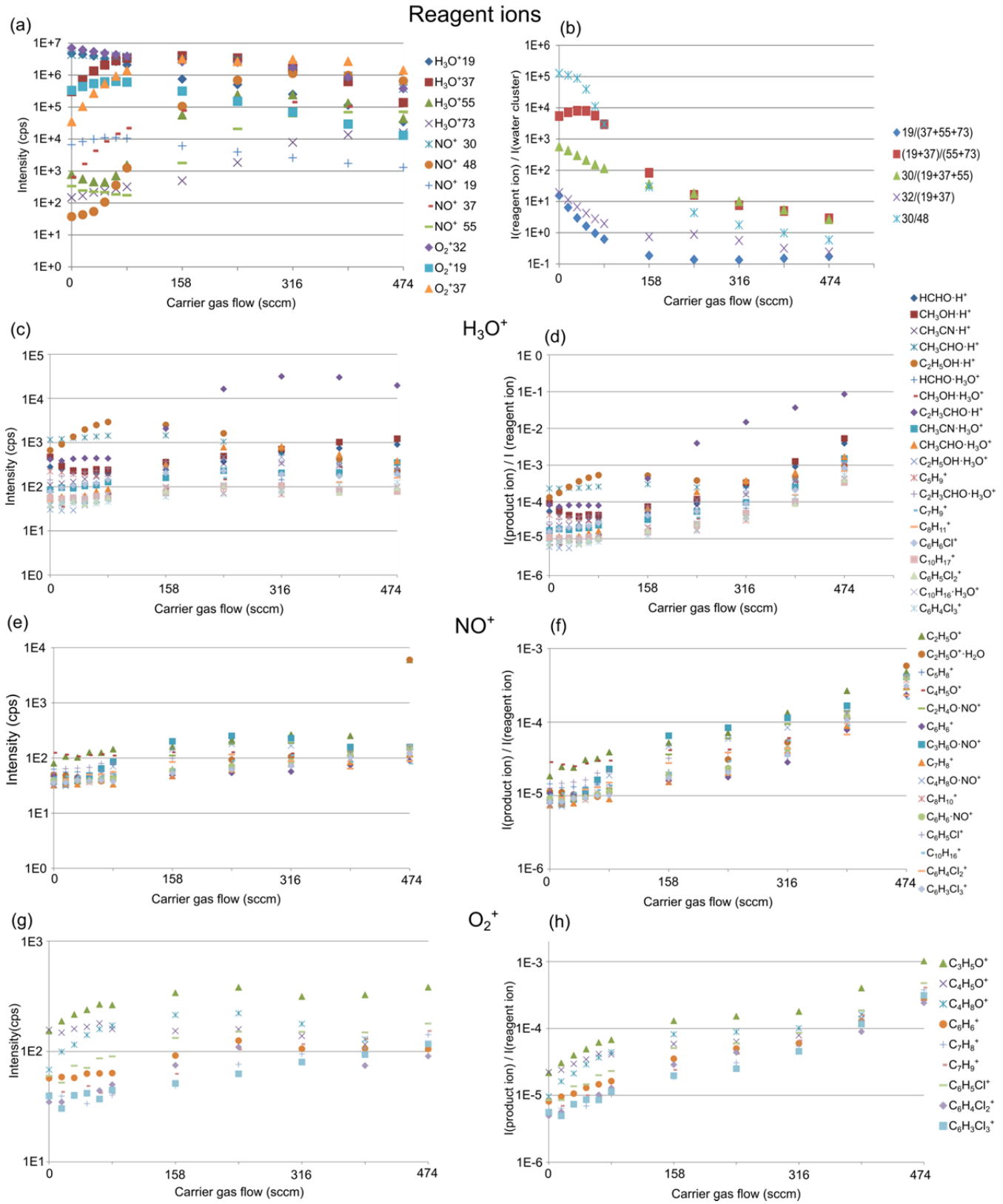

Figure S11: Carrier gas flow optimization for nitrogen carrier gas and zero air dilution gas, U_{FT} = 50 V, T_{FT} = 140°C, 90% humidity at 25°C. (a–b) for the different reagent ions H_3O^+, NO^+, and O_2^+, the detected primary and secondary reagent ions symbolized by their mass are shown 19 = H_2O^+, 37 = $H_3O^+ \cdot H_2O$, 55 = $H_3O^+ \cdot 2\ H_2O$, 73 = $H_3O^+ \cdot 3\ H_2O$, 30 = NO^+, 48 = $NO^+ \cdot H_2O$, 32 = O_2^+. (a) absolute ion counts, (b) proportion of reagent ions relative to the water clusters. (c–h) behaviour of the product ions upon reaction with H_3O^+ (19 + 37 + 55, c, d), NO^+ (e, f), and O_2^+ (g, h) as reagent ions. (c, e, g) absolute ion counts, (d, f, h) counts normalized to reagent ion counts.

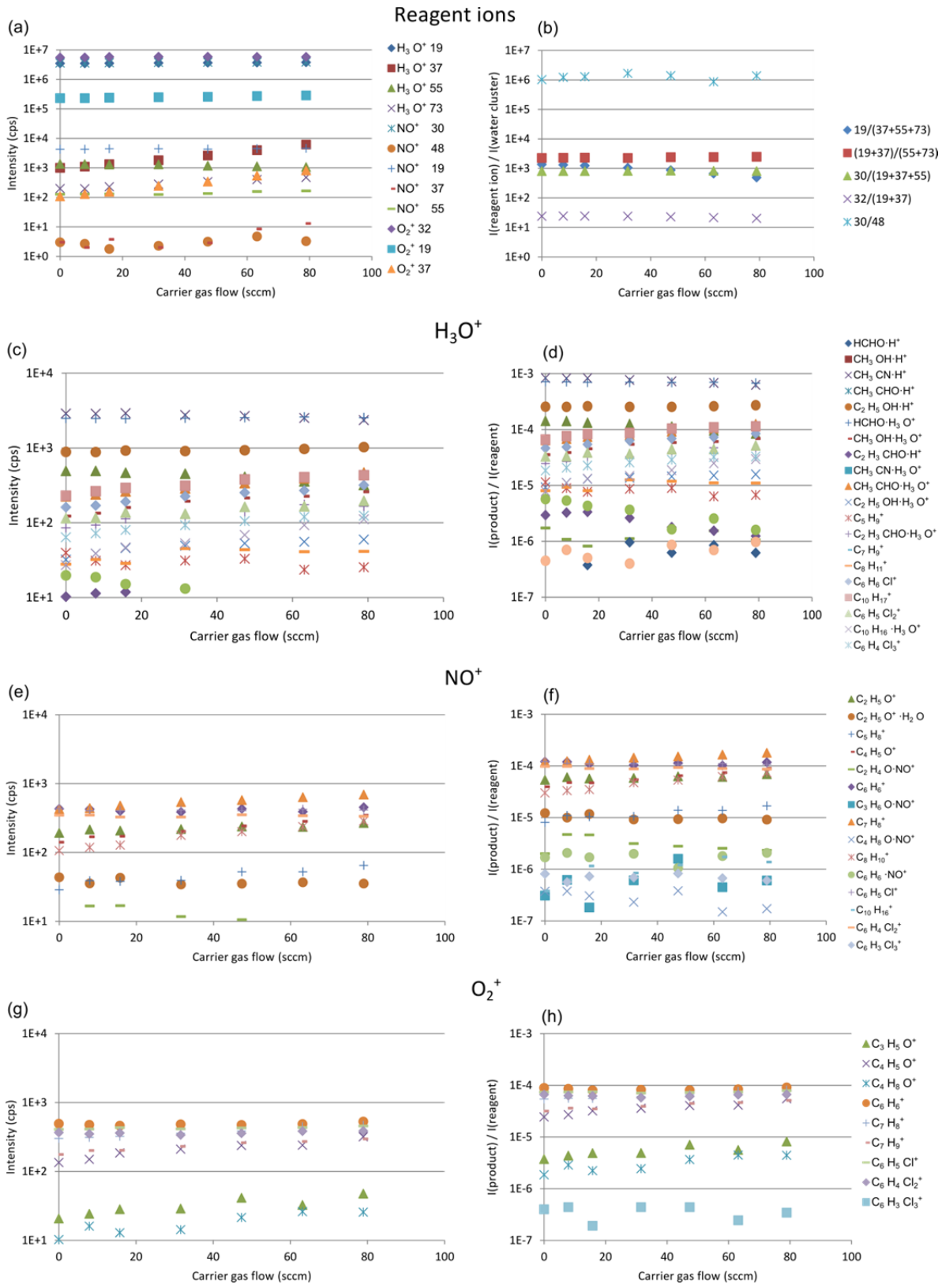

Figure S12: Carrier gas flow optimization for nitrogen carrier gas and zero air dilution gas, U_{FT} = 50 V, T_{FT} = 140°C, 90% humidity at 25°C, picture section of Fig. S11 for low carrier gas flows. (a–b) for the different reagent ions H_3O^+, NO^+, and O_2^+, the detected primary and secondary reagent ions symbolized by their mass are shown 19 = H_2O^+, 37 = $H_3O^+ \cdot H_2O$, 55 = $H_3O^+ \cdot 2\ H_2O$, 73 = $H_3O^+ \cdot 3\ H_2O$, 30 = NO^+, 48 = $NO^+ \cdot H_2O$, 32 = O_2^+. (a) absolute ion counts, (b) proportion of reagent ions relative to the water clusters. (c–h) behaviour of the product ions upon reaction with H_3O^+ (19 + 37 + 55, c, d), NO^+ (e, f), and O_2^+ (g, h) as reagent ions. (c, e, g) absolute ion counts, (d, f, h) counts normalized to reagent ion counts.

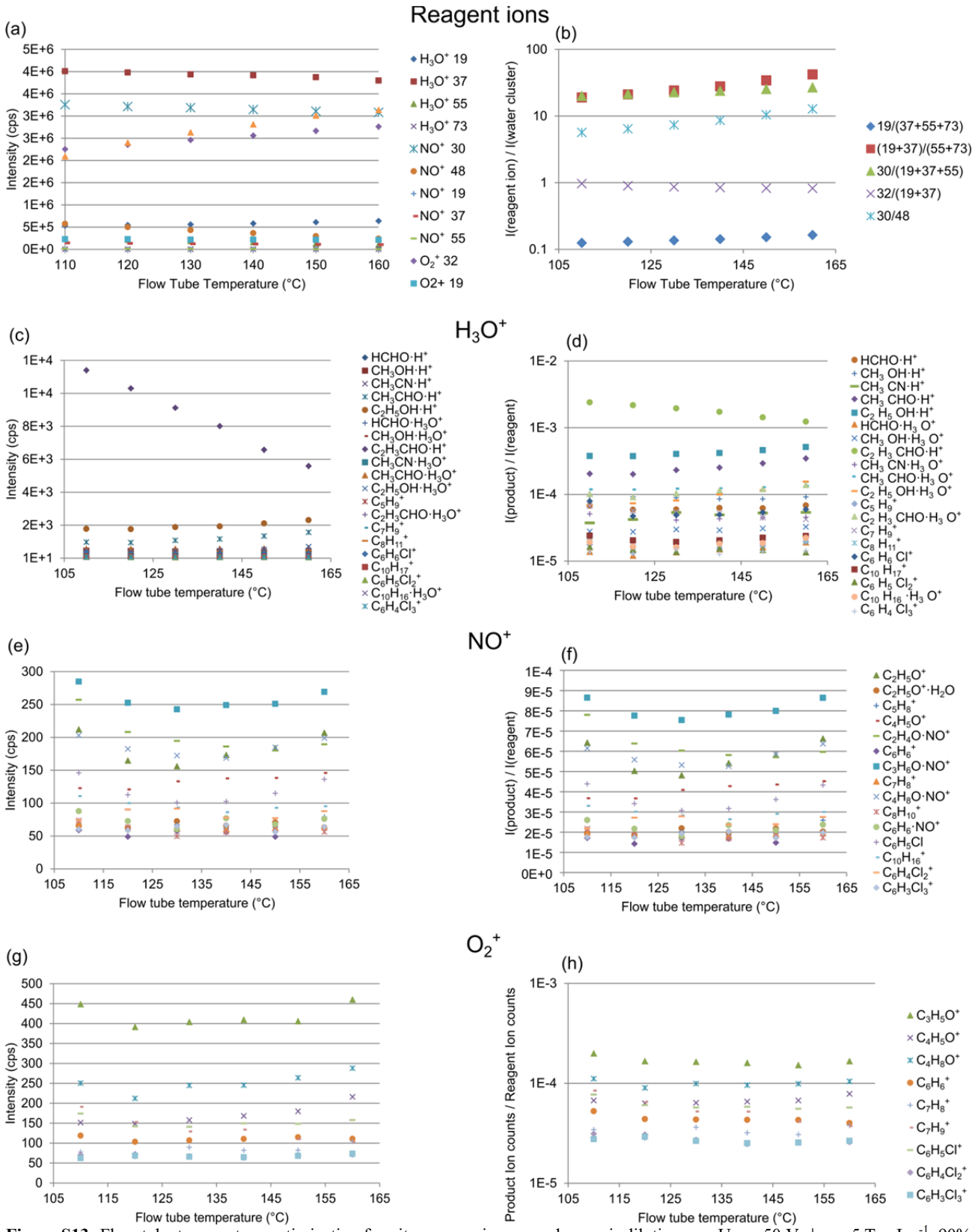

Figure S13: Flow tube temperature optimization for nitrogen carrier gas and zero air dilution gas, U_{FT} = 50 V, ϕ_{FT} = 5 TorrL s^{-1}, 90% humidity at 25°C. (a–b) for the different reagent ions H_3O^+, NO^+, and O_2^+, the detected primary and secondary reagent ions symbolized by their mass are shown 19 = H_2O^+, 37 = $H_3O^+ \cdot H_2O$, 55 = $H_3O^+ \cdot 2\ H_2O$, 73 = $H_3O^+ \cdot 3\ H_2O$, 30 = NO^+, 48 = $NO^+ \cdot H_2O$, 32 = O_2^+. (a) absolute ion counts, (b) proportion of reagent ions relative to the water clusters. (c–h) behaviour of the product ions upon reaction with H_3O^+ (19 + 37 + 55, c, d), NO^+ (e, f), and O_2^+ (g, h) as reagent ions. (c, e, g) absolute ion counts, (d, f, h) counts normalized to reagent ion counts.

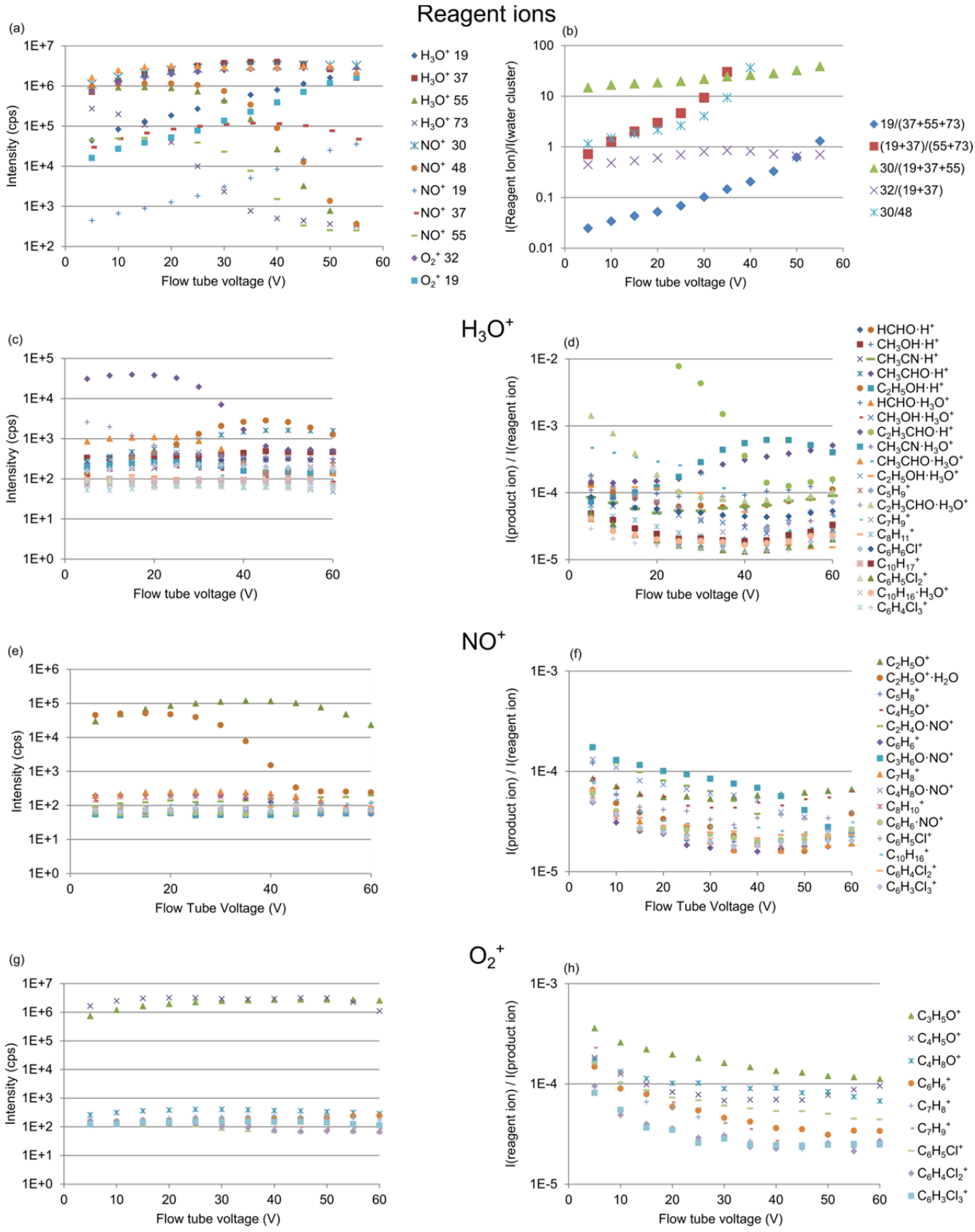

Figure S14: Flow tube voltage optimization for nitrogen carrier gas and zero air dilution gas, ϕ_{FT} = 5 TorrL s^{-1}, T_{FT} = 140°C, 90% humidity at 25°C. (a–b) for the different reagent ions H_3O^+, NO^+, and O_2^+, the detected primary and secondary reagent ions symbolized by their mass are shown 19 = H_2O^+, 37 = $H_3O^+ \cdot H_2O$, 55 = $H_3O^+ \cdot 2\ H_2O$, 73 = $H_3O^+ \cdot 3\ H_2O$, 30 = NO^+, 48 = $NO^+ \cdot H_2O$, 32 = O_2^+. (a) absolute ion counts, (b) proportion of reagent ions relative to the water clusters. (c–h) behaviour of the product ions upon reaction with H_3O^+ (19 + 37 + 55, c, d), NO^+ (e, f), and O_2^+ (g, h) as reagent ions. (c, e, g) absolute ion counts, (d, f, h) counts normalized to reagent ion counts.

Table S1: LODs (in ppb, derived from Blank, 3*sd), of the SIFT-MS with nitrogen carrier gas of the different compounds and relative humidities at 25°C.

compound	m/z_{reag} / m/z_{prod}	Dry	30% humidity	60% humidity	90% humidity
methanol	19 / 33	0.720	0.342	0.385	0.803
acetonitrile	19 / 42	0.075	0.053	0.063	0.251
acetaldehyde	19 / 45	0.429	0.288	0.240	0.281
acrolein	19 / 57	0.112	0.219	0.348	1.077
isoprene	19 / 69	0.120	0.142	0.167	0.264
butanone	19 / 73	0.112	0.191	0.152	0.229
toluene	19 / 93	0.048	0.164	0.100	0.222
o-xylene	19 / 107	0.074	0.126	0.193	0.272
a-pinene	19 / 137	0.317	0.064	0.319	0.168
dichlorobenzene	19 / 147	0.131	0.120	0.196	2.609
isoprene	30 / 68	0.094	0.110	0.141	0.182
2-butenal	30 / 69	0.084	0.077	0.033	0.060
benzene	30 / 78	0.063	0.181	0.098	0.215
toluene	30 / 92	0.127	0.058	0.094	0.098
butanone	30 / 102	0.116	0.093	0.116	0.114
***o*-xylene**	30 / 106	0.073	0.212	0.106	0.090
chlorobenzene	30 / 112	0.145	0.193	0.238	0.219
α-pinene	30 / 136	0.125	0.240	0.292	0.359
dichlorobenzene	30 / 146	0.175	0.144	0.155	0.239
2-butenal	32 / 69	0.026	0.177	0.166	0.181
butanone	32 / 72	0.113	0.140	0.192	0.460
benzene	32 / 78	0.080	0.109	0.064	0.136
toluene	32 / 92	0.066	0.050	0.081	0.087
α-pinene	32 / 93	0.049	0.088	0.130	0.214
chlorobenzene	32 / 112	0.132	0.219	0.079	0.192
dichlorobenzene	32 / 146	0.194	0.093	0.117	0.171

Table S2: Sensitivities ± 95% confidence interval (in cps/ppb, based on product ion counts normalized to 10^6 reagent ion counts, df = 26), of the SIFT-MS with nitrogen carrier gas of the different compounds and relative humidities at 25°C. NA: LOD was over 2 ppb so that not enough calibration points remained for a calibration.

compound	m/z_{reag} / m/z_{prod}	Dry	30% humidity	60% humidity	90% humidity
methanol	19 / 33	111 ± 2	104 ± 2	110 ± 2	36.2 ± 0.8
acetonitrile	19 / 42	235 ± 2	236 ± 1	232 ± 2	109.0 ± 0.8
acetaldehyde	19 / 45	200 ± 2	195 ± 2	194 ± 2	85 ± 1
acrolein	19 / 57	220 ± 4	223 ± 3	219 ±3	118 ± 3
isoprene	19 / 69	135 ± 1	129 ± 1	124 ± 2	29.8 ± 0.4
butanone	19 / 73	264 ± 1	252 ± 2	250 ± 2	148 ± 2
toluene	19 / 93	137 ± 1	130.2 ± 0.9	127 ± 1	21.5 ± 0.7
o-xylene	19 / 107	144.4 ± 0.8	137.2 ± 0.9	135 ± 1	28.4 ± 0.3
a-pinene	19 / 137	63.1 ± 0.6	63.4 ± 0.9	59.0 ± 0.6	36.1 ± 0.5
dichlorobenzene	19 / 147	71.0 ± 0.9	64.1 ± 0.6	62.8 ± 0.8	3.4 ± 0.3
isoprene	30 / 68	82.9 ± 0.9	83.2 ± 0.8	79.6 ± 0.8	71.1 ± 0.6
2-butenal	30 / 69	204 ± 2	201 ± 2	194 ± 1	186 ± 3
benzene	30 / 78	71.6 ± 0.6	72.3 ± 0.7	67.3 ± 0.9	60.3 ± 0.6
toluene	30 / 92	131.7 ± 0.8	134 ± 1	125 ± 1	115.9 ± 0.5
butanone	30 / 102	130 ± 1	127.0 ± 0.9	121.0 ± 0.8	130 ± 2
***o*-xylene**	30 / 106	114 ± 0.8	111 ± 1	106 ± 1	103.5 ± 0.9
chlorobenzene	30 / 112	87.8 ± 0.9	86 ± 1	80.1 ± 0.7	75 ± 1
α-pinene	30 / 136	61.4 ± 0.5	60.4 ± 0.9	56.1 ± 0.7	62.1 ± 0.9
dichlorobenzene	30 / 146	60.0 ± 0.7	59.2 ± 0.7	56.2 ± 0.6	48.6 ± 0.9
2-butenal	32 / 69	136 ± 1	132.2 ± 0.9	128 ± 1	109 ± 2
butanone	32 / 72	51.5 ± 0.5	50.9 ± 0.7	48.6 ± 0.7	60.1 ± 0.9
benzene	32 / 78	88.8 ± 0.6	86.4 ± 0.5	85.3 ± 0.7	108.8 ± 0.7
toluene	32 / 92	113.6 ± 0.7	112.1 ± 0.8	104.9 ± 0.7	133.9 ± 0.7
α-pinene	32 / 93	64.6 ± 0.6	66.2 ± 0.5	62.1 ± 0.4	80 ± 1
chlorobenzene	32 / 112	75.0 ± 0.8	74 ± 1	72.6 ± 0.7	89 ± 1
dichlorobenzene	32 / 146	54.2 ± 0.5	53.2 ± 0.7	48.3 ± 0.5	62.0 ± 0.7

Table S3: SNR at 1 ppb ± 95% upper and lower confidence interval (CI^u and CI^l), based on product ion counts normalized to 10^6 reagent ion counts, df = 7) of the SIFT-MS with nitrogen carrier gas of the different compounds and relative humidities at 25°C. NA: LOD was over 2 ppb so that not enough calibration points remained for a calibration.

compound	m/z_{reag} / m/z_{prod}	**dry**			**30% humidity**			**60% humidity**			**90% humidity**		
		SNR	CI^u	CI^l	SNR	CI^u	CI^l	SNR	CI^u	CI^l	SNR	CI^u	CI^l
methanol	19 / 33	1.6	0.7	0.5	1.9	0.4	0.4	1.7	0.5	0.4	1.8	0.6	0.4
acetonitrile	19 / 42	6.6	3.0	2.2	8.6	3.8	2.9	5.4	1.5	1.2	3.6	2.6	1.5
acetaldehyde	19 / 45	1.6	0.4	0.3	1.3	0.2	0.2	1.4	0.2	0.2	1.4	0.2	0.2
acrolein	19 / 57	5.4	1.2	1.1	2.6	0.5	0.4	2.0	0.5	0.5	1.1	0.1	0.1
isoprene	19 / 69	6.7	5.1	3.1	5.3	2.9	2.0	5.1	3.5	2.2	2.6	1.7	1.2
butanone	19 / 73	3.6	1.0	0.9	2.3	0.7	0.6	2.6	0.5	0.4	1.5	0.3	0.3
toluene	19 / 93	8.3	2.1	1.7	6.6	6.0	3.4	6.4	2.8	2.0	3.4	1.3	1.1
o-xylene	19 / 107	7.4	3.3	2.5	5.8	2.7	1.9	5.3	4.7	2.7	2.1	0.9	0.7
a-pinene	19 / 137	5.4	6.4	3.2	5.1	0.9	0.8	3.5	3.2	2.0	2.5	0.8	0.6
dichlorobenzene	19 / 147	5.5	4.1	2.7	5.2	2.7	2.0	4.8	4.7	3.0	1.5	1.3	0.9
isoprene	30 / 68	6.4	3.6	2.7	5.1	2.7	2.0	6.2	4.6	3.0	4.6	2.7	1.7
2-butenal	30 / 69	6.6	5.0	3.0	5.7	1.9	1.5	5.8	1.0	0.9	1.8	1.0	0.8
benzene	30 / 78	3.9	1.1	1.0	4.4	3.0	2.0	4.4	1.7	1.4	4.8	4.5	2.5
toluene	30 / 92	8.2	8.7	4.7	9.4	4.5	3.3	7.3	4.3	2.9	6.4	3.9	2.7
butanone	30 / 102	4.3	2.1	1.5	4.1	1.2	1.0	3.6	1.0	0.8	2.3	1.1	0.9
***o*-xylene**	30 / 106	5.4	1.7	1.4	5.1	5.2	2.9	5.3	3.2	2.3	6.0	3.6	2.5
chlorobenzene	30 / 112	4.5	1.5	1.1	3.8	2.0	1.5	3.9	2.3	1.6	3.6	2.6	1.7
α-pinene	30 / 136	4.6	1.5	1.2	5.4	4.2	2.6	3.5	2.9	1.9	3.5	2.9	1.6
dichlorobenzene	30 / 146	5.9	4.3	2.6	5.4	3.5	2.5	4.6	2.7	2.0	3.0	1.5	1.1
2-butenal	32 / 69	4.2	1.0	0.9	3.7	1.9	1.4	3.9	1.9	1.3	1.7	1.0	0.8
butanone	32 / 72	3.4	0.7	0.7	1.9	0.3	0.3	2.2	0.5	0.4	1.6	0.7	0.5
benzene	32 / 78	5.5	3.2	2.4	6.9	4.1	2.8	5.0	1.2	1.0	3.4	1.2	0.9
toluene	32 / 92	9.1	3.8	2.7	7.5	2.4	1.9	7.3	4.8	3.5	6.4	3.8	2.7
α-pinene	32 / 93	5.8	1.6	1.4	4.9	1.7	1.4	4.4	2.3	1.7	3.7	1.7	1.2
chloro-benzene	32 / 112	5.0	2.6	2.0	3.7	2.3	1.6	3.3	0.8	0.7	2.7	1.0	0.8
dichloro-benzene	32 / 146	5.5	5.1	2.8	7.3	4.2	3.1	5.1	2.6	1.9	3.4	2.1	1.6

S2 Humidity dependence of product ion intensities of the SIFT-MS

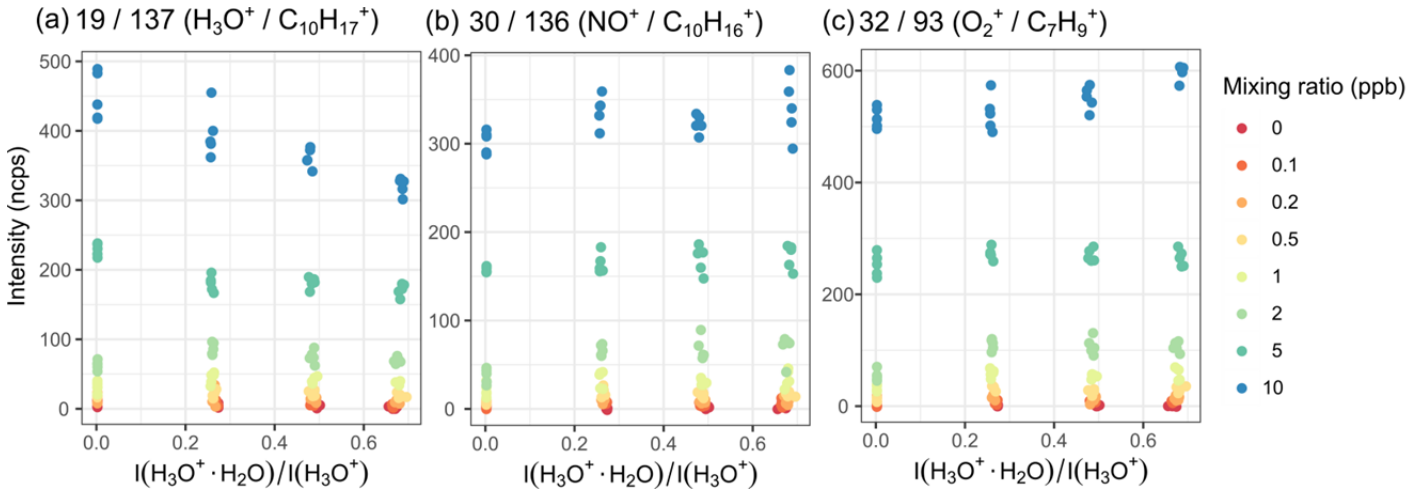

Figure S15: Humidity dependence of α-pinene signal at mixing ratios between 0.1 and 10 ppb upon reaction with the different reagent ions H_3O^+ (a), NO^+ (b), and O_2^+ (c) forming the product ions $C_{10}H_{17}^+$, $C_{10}H_{16}^+$, and $C_7H_9^+$. Humidity is measured as the ratio of the $H_3O^+ \cdot H_2O$ and the H_3O^+ intensity, cf. Fig. S20.

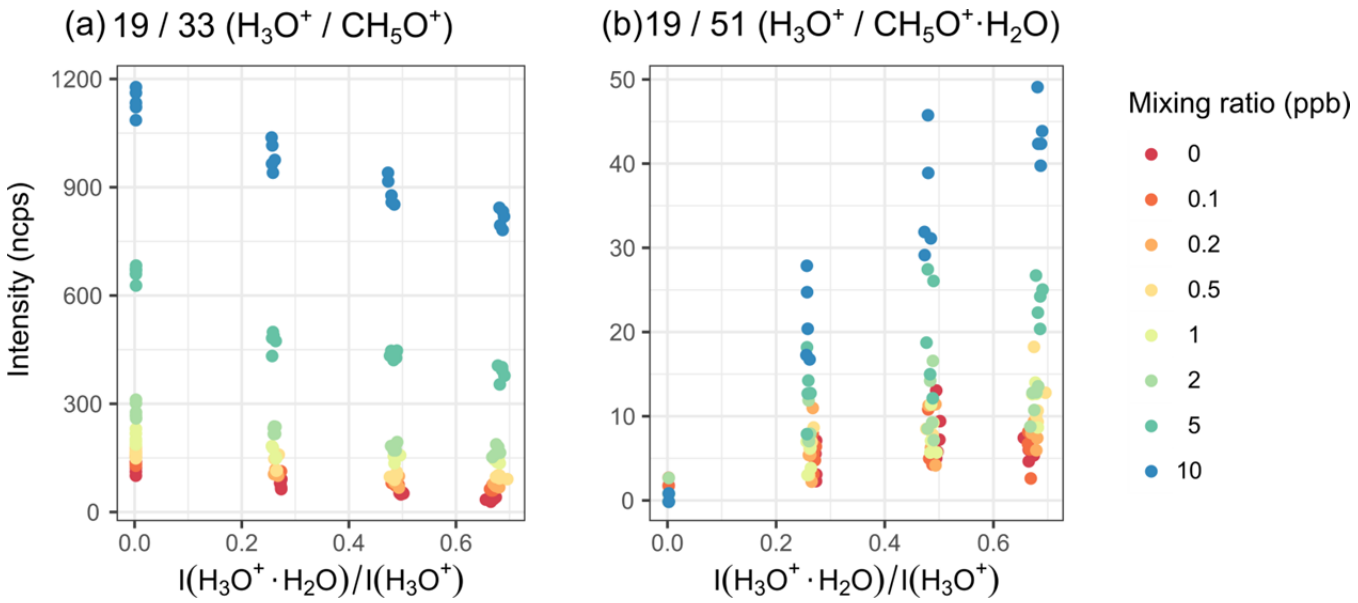

Figure S16: Humidity dependence of methanol signal, $CH_3OH_2^+$ (19 / 33) (a) and its first water cluster, $CH_3OH \cdot H_3O^+$ (19 / 51) (b). Humidity is measured as the ratio of the $H_3O^+ \cdot H_2O$ and the H_3O^+ intensity, cf. Fig. S20.

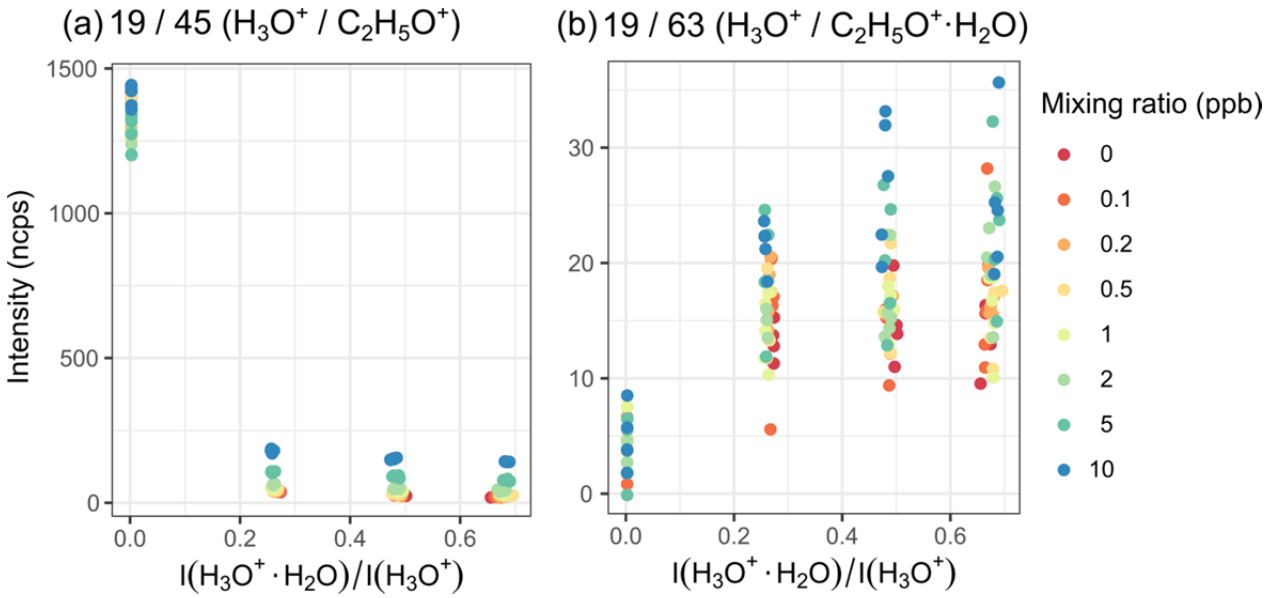

Figure S17: Humidity dependence of acetaldehyde (19/45) (a) and its water cluster (19/63) (b). Humidity is measured as the ratio of the $H_3O^+ \cdot H_2O$ and the H_3O^+ intensity, cf. Fig. S20.

In dry air, m/z = 45 amu shows a very high background. In dry state there is a very high background that does not occur when the system is wet. It cannot be found when reacting with NO^+, but the reaction is roughly five times slower, so that the intensity is not high enough to detect acetaldehyde via this reaction. The background might either be due to the transfer line bypassing the water bubbler in dry state or desorption of a compound forming m/z = 45 when all the surfaces are dry.

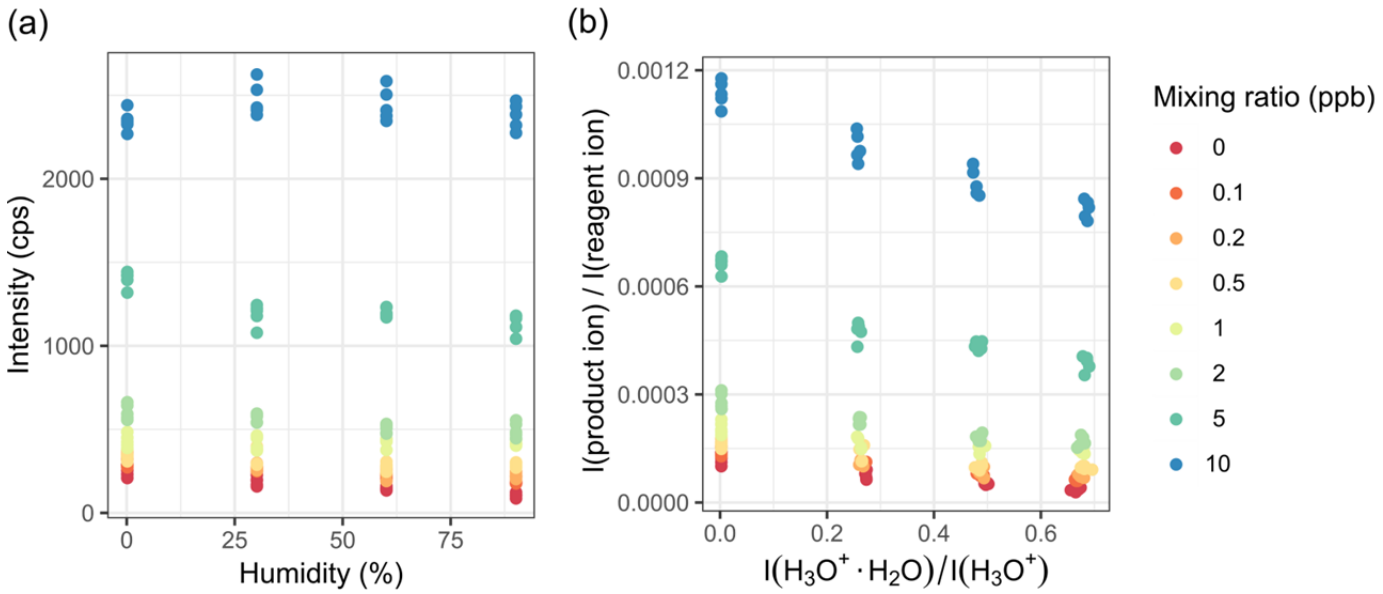

Figure S18: Humidity dependence of methanol m/z = 33 amu intensity. (a) Absolute counts vs. relative humidity at 25°C. (b) Relative intensity per reagent intensity vs. the ratio of H_3O^+ and its first water cluster as a measure of humidity.

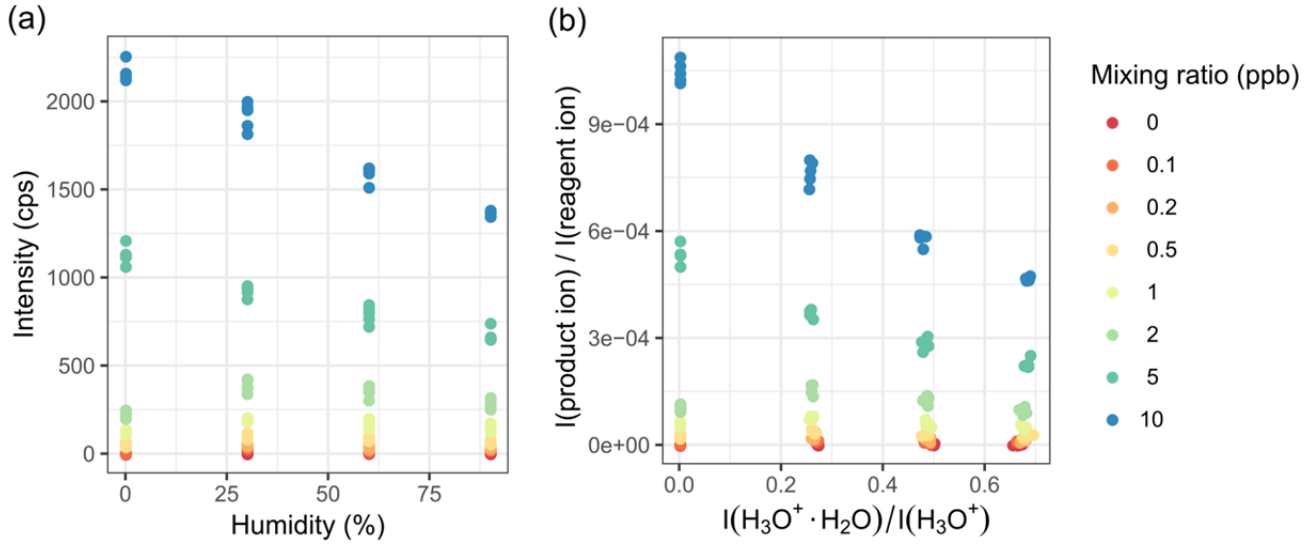

Figure S19: Humidity dependence of toluene (*m*/*z* = 93 u) intensity. (a) Absolute counts vs. relative humidity at 25°C. (b) Relative intensity per reagent intensity vs. the ratio of H_3O^+ and its first water cluster as a measure of humidity.

At mixing ratios smaller than 2 ppb, none of the plots is linear for the dry state.

S3 Evaluation of calibration procedures

Table S4: Compounds and their ions evaluated for the calibration.

reagent ion	*m*/*z* (u)	compound	product ion
H_3O^+	33	methanol	CH_5O^+
H_3O^+	42	acetonitrile	CH_4CN^+
H_3O^+	45	acetaldehyde	$C_2H_5O^+$
H_3O^+	47	ethanol	$C_2H_7O^+$
H_3O^+	51	methanol	$CH_3OH_2^+ \cdot H_2O$
H_3O^+	57	acrolein	$C_3H_5O^+$
H_3O^+	60	acetonitrile	$CH_4CN^+ \cdot H_2O$
H_3O^+	63	acetaldehyde	$C_2H_5O^+ \cdot H_2O$
H_3O^+	65	ethanol	$C_2H_7O^+ \cdot H_2O$
H_3O^+	69	isoprene	$C_5H_9^+$
H_3O^+	75	acrolein	$C_3H_5O^+ \cdot H_2O$
H_3O^+	93	toluene	$C_7H_9^+$
H_3O^+	107	*o*-xylene	$C_8H_{11}^+$
H_3O^+	113	chlorobenzene	$C_6H_6{}^{35}Cl^+$
H_3O^+	137	α-pinene	$C_{10}H_{17}^+$
H_3O^+	147	1, 4-dichlorobenzene	$C_6H_5{}^{35}Cl_2^+$
NO^+	45	ethanol	$C_2H_5O^+$
NO^+	55	acrolein	$C_3H_3O^+$
NO^+	63	ethanol	$C_2H_5O^+ \cdot H_2O$
NO^+	68	isoprene	$C_5H_8^+$
NO^+	69	2-butenal	$C_4H_5O^+$
NO^+	74	acetaldehyde	$C_2H_4O \cdot NO^+$
NO^+	78	benzene	$C_6H_6^+$
NO^+	88	acetone	$C_3H_6O \cdot NO^+$
NO^+	92	toluene	$C_7H_8^+$
NO^+	102	butanone	$C_4H_8O \cdot NO^+$
NO^+	106	*o*-xylene	$C_8H_{10}^+$
NO^+	108	benzene	$C_6H_6 \cdot NO^+$
NO^+	112	chlorobenzene	$C_6H_5{}^{35}Cl^+$
NO^+	136	α-pinene	$C_{10}H_{16}^+$
NO^+	146	1, 4-dichlorobenzene	$C_6H_4{}^{35}Cl_2^+$
O_2^+	39	benzene	$CH_3O^+ \cdot H_2O$
O_2^+	58	acetone	$C_3H_5O^+$
O_2^+	69	2-butenal	$C_4H_5O^+$
O_2^+	72	butanone	$C_4H_8O^+$
O_2^+	78	benzene	$C_6H_6^+$
O_2^+	92	toluene	$C_7H_8^+$
O_2^+	93	α-pinene	$C_7H_9^+$
O_2^+	112	chlorobenzene	$C_6H_5{}^{35}Cl^+$
O_2^+	146	1, 4-dichlorobenzene	$C_6H_4{}^{35}Cl_2^+$

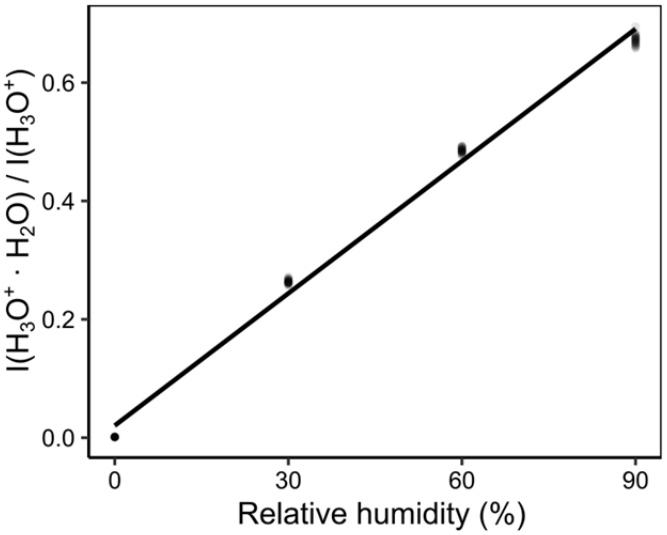

Figure S20: Correlation of the intensity ratio of the reagent ion water clusters with the relative humidity. The results are not entirely linear, but the deviance is so small that they were approximated linearly.

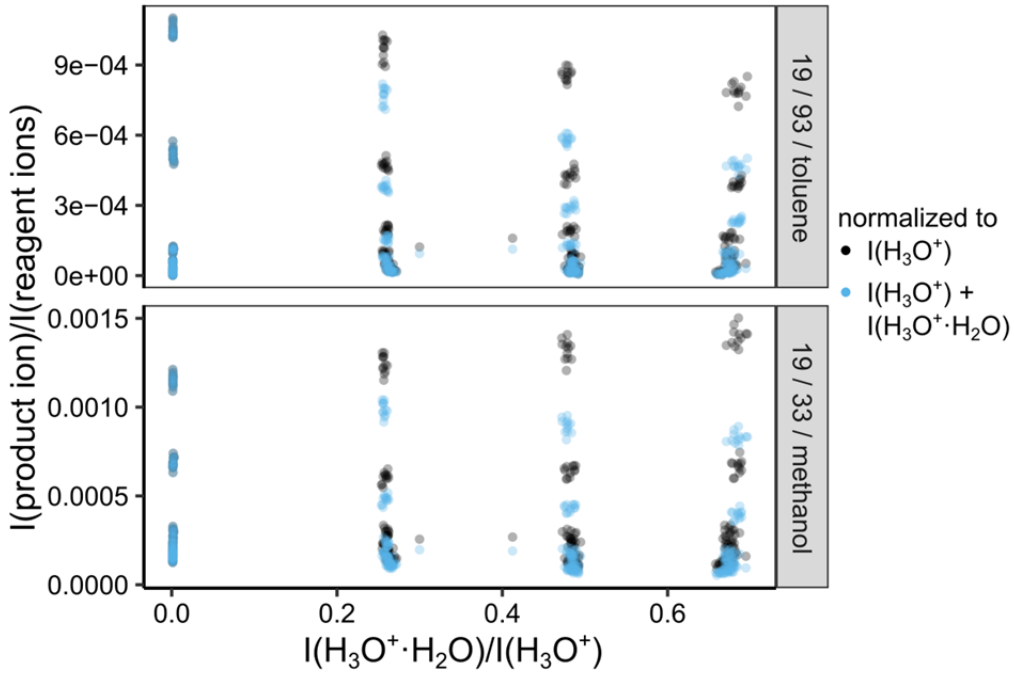

Figure S21: Effect of normalization to H_3O^+ vs. to both H_3O^+ and $H_3O^+ \cdot H_2O$. The latter makes the data more humidity dependent, but it accounts for effects seen for methanol, where a drop in H_3O^+ leads to a pseudo signal increase if not corrected for the first water cluster.

Table S5: Bayesian Information Criteria (BIC) of the different substances and their mean, median, minimum and maximum value for the different regression methods, named by the equations numbers they were calculated on. Equation (6) was not calculated for the reagent ions separately, but for the total mixing ratio result of the substance.

substance	ion	Eq. (2) dry	Eq. (2) 30%	Eq. (2) 60%	Eq. (2) 90%	Eq. (3) dry	Eq. (3) 30%	Eq. (3) 60%	Eq. (3) 90%	Eq. (4)	Eq. (5)	Eq. (6)	Eq. (7)	Eq. (8)	Eq. (9)
methanol	19 / 33	236	361	408	302	348	433	627	442	101	192	921	103	101	103
acetonitrile	19 / 42	462	402	407	416	557	632	628	625	4	231	33	18	0	18
acetaldehyde	19 / 45		298	298	290		437	447	455	3	64	2045	40	0	40
ethanol	19 / 47	475	387	403	175	387	499	634	273	349	298	1664		395	
acrolein	19 / 57	400	418	397	290	473	615	641	453	59	260	1071	23	57	23
isoprene	19 / 69	369	376	320	351	507	663	571	689	208	348	235	65	68	65
2-butanone	19 / 73	394	411	399	277	478	626	641	467	15	220	128	33	62	33
toluene	19 / 93	362	358	346	317	511	671	694	724	301	423	267	57	73	57
***o*-xylene**	19 / 107	243	373	308	263	340	655	478	480	190	297	467	69	101	69
chlorobenzene	19 / 113	288	301	250	197	441	583	493	397	267	344	336	98	102	98
α-pinene	19 / 137	216	323	319	275	369	563	721	620	115	218	2218	106	128	106
dichlorobenzene	19 / 147	274	283	295	308	453	601	744	734	418	483		132	253	132
ethanol	30 / 45		224	211	262		362	370	464	213	220			266	
acrolein	30 / 55	230	356	336	195	353	660	681	391	220	229		266	73	266
isoprene	30 / 68	346	330	340	355	524	695	680	671	65	71		73	112	73
2-butenal	30 / 69	383	405	337	241	486	621	529	338	64	57		62	343	62
benzene	30 / 78	336	345	307	320	537	675	559	557	101	94		92	198	92
acetone	30 / 88	146	242	218	191	291	488	511	395	181	164		198	38	198
toluene	30 / 92	369	349	361	363	502	669	659	656	27	32		38	62	38
butanone	30 / 102	222	287	252	303	355	585	479	566	96	93		112	35	112
***o*-xylene**	30 / 106	393	338	330	371	621	675	691	659	42	25		35		35
benzene	30 / 108	170	135	176	162	410	302	405	420	234	234			124	

chlorobenzene	30 / 112	331	261	258	368	541	468	465	654	119	126		124	147	124
α-pinene	30 / 136	282	316	271	253	590	705	602	470	148	127		23	136	23
dichlorobenzene	30 / 146	313	289	333	307	555	585	686	562	141	136		136	163	136
acetone	32 / 58	155				288				152	151		163	245	163
2-butenal	32 / 69	246	284	277	266	349	459	455	462	250	200		246		246
butanone	32 / 72	170	203	258	206	277	388	474	374	118	103			112	
benzene	32 / 78	353	350	355	292	530	686	682	583	78	44		112	68	112
toluene	32 / 92	357	353	368	380	527	672	659	639	107	46		67	68	67
α-pinene	32 / 93	330	364	331	352	554	679	694	667	94	91		48	73	48
chlorobenzene	32 / 112	271	282	250	304	469	610	482	563	91	48		73	142	73
dichlorobenzene	32 / 146	318	343	324	289	567	697	692	584	122	124		142	134	142
mean		305	323	314	289	458	583	587	532	142	175	853	95	125	95
median		318	341	322	291	478	618	628	560	118	151	467	73	102	73
min		146	135	176	162	277	302	370	273	3	25	33	18	35	18
max		475	418	408	416	621	705	744	734	418	483	2218	266	395	266

S4 Comparison of SIFT-MS to PTR-MS

Table S6: LODs (in ppb, derived from Blank, 3*sd) of the PTR-MS of the different compounds for the different humidities at 25°C. n.d.: intensities were not measured at this *m/z* and humidity.

Compound	m/z	dry	30% humidity	60% humidity	90% humidity
methanol	33	0.618	0.681	0.685	0.835
acetonitrile	42	0.026	0.020	n.d.	n.d.
acetaldehyde	45	0.266	0.188	n.d.	n.d.
acrolein	57	0.055	0.051	n.d.	n.d.
acetone	59	0.043	0.049	0.029	0.028
isoprene	69	0.070	0.061	0.065	0.159
2-butenal	71	0.024	0.015	0.024	0.034
butanone	73	0.095	0.033	0.072	0.072
benzene	79	0.066	0.060	0.019	0.026
toluene	93	0.137	0.110	0.077	0.071
***o*-xylene**	107	0.061	0.107	n.d.	n.d.
α-pinene	137	0.049	0.025	0.050	0.037
dichlorobenzene	148	0.000	0.150	n.d.	n.d.

Table S7: LODs (in ppb, derived from Blank, 3*sd), of the SIFT-MS with Helium carrier gas of the different compounds and relative humidities at 25°C.

compound	m/z_{reag} / m/z_{prod}	LOD (ppb)			
		dry	30% humidity	60% humidity	90% humidity
methanol	19 / 33	>2	1.047	>2	1.367
acetonitrile	19 / 42	0.111	0.133	0.081	0.139
acetaldehyde	19 / 45	1.315	0.934	0.999	0.852
acrolein	19 / 57	0.332	0.382	0.341	0.281
acetone	19 / 59	0.378	0.347	0.501	0.416
isoprene	19 / 69	0.460	0.333	0.318	0.434
2-butenal	19 / 71	0.176	0.093	0.159	0.109
butanone	19 / 73	0.142	0.186	0.126	0.164
benzene	19 / 79	0.107	0.132	0.195	0.171
toluene	19 / 93	0.072	0.124	0.120	0.154
***o*-xylene**	19 / 107	0.093	0.064	0.106	0.100
α-pinene	19 / 137	0.088	0.091	0.147	0.078
dichlorobenzene	19 / 147	0.047	0.066	0.138	0.195
isoprene	30 / 68	0.189	0.337	0.242	0.175
2-butenal	30 / 69	0.171	0.121	0.117	0.136
benzene	30 / 78	0.082	0.081	0.080	0.070
toluene	30 / 92	0.031	0.026	0.025	0.027
butanone	30 / 102	0.452	0.497	0.390	0.393
***o*-xylene**	30 / 106	0.098	0.039	0.074	0.074
chlorobenzene	30 / 112	0.091	0.157	0.137	0.124
α-pinene	30 / 136	0.489	0.398	0.498	0.457
dichlorobenzene	30 / 146	0.057	0.066	0.065	0.051
2-butenal	32 / 69	0.217	0.239	0.250	0.249
butanone	32 / 72	0.652	0.455	0.866	0.528
benzene	32 / 78	0.151	0.117	0.151	0.118
toluene	32 / 92	0.084	0.063	0.091	0.063
α-pinene	32 / 93	0.098	0.080	0.121	0.144
chlorobenzene	32 / 112	0.122	0.097	0.087	0.128
dichlorobenzene	32 / 146	0.079	0.038	0.087	0.078

Table S8: Sensitivities ± 95% confidence interval (in cps/ppb, based on product ion counts normalized to 10^6 reagent ion counts, df = 26) of the PTR-MS of the different compounds for the different humidities at 25°C. n.d.: intensities were not measured at this *m/z* and humidity.

compound	m/z	sensitivity ± 95% CI (cps/ppb)			
		dry	30% humidity	60% humidity	90% humidity
methanol	33	14.3 ± 0.6	14.3 ± 0.4	12.2 ± 0.2	9.2 ± 0.4
acetonitrile	42	25.5 ± 0.4	25.1 ± 0.3	n.d.	n.d.
acetaldehyde	45	21.4 ± 0.3	20.9 ± 0.3	n.d.	n.d.
acrolein	57	19 ± 1	21.4 ± 0.3	n.d.	n.d.
acetone	59	28.8 ± 0.4	27.8 ± 0.3	26.2 ± 0.2	24.7 ± 0.4
isoprene	69	9.39 ± 0.05	10.60 ± 0.03	4.22 ± 0.04	4.17 ± 0.02
2-butenal	71	31 ± 1	32.4 ± 0.4	14.9 ± 0.2	12.8 ± 0.3
butanone	73	28 ± 1	28.4 ± 0.3	16.2 ± 0.2	14.1 ± 0.3
benzene	79	17.0 ± 0.3	16.7 ± 0.3	n.d.	n.d.
toluene	93	20.1 ± 0.3	19.0 ± 0.2	15.8 ± 0.1	16.7 ± 0.3
o-xylene	107	22.6 ± 0.2	21.6 ± 0.3	n.d.	n.d.
a-pinene	137	8.2 ± 0.2	8.5 ± 0.1	6.08 ± 0.07	6.1 ± 0.2
dichlorobenzene	148	0.90 ± 0.04	0.84 ± 0.04	n.d.	n.d.

Table S9: Sensitivities ± 95% confidence interval (in cps/ppb, based on product ion counts normalized to 10^6 reagent ion counts, df = 26), of the SIFT-MS of the different compounds and relative humidities at 25°C. NA: LOD was over 2 ppb so that not enough calibration points remained for a calibration.

compound	m/z_{reag} / m/z_{prod}	**sensitivity ± 95% CI (cps/ppb)**			
		dry	**30% humidity**	**60% humidity**	**90% humidity**
methanol	19 / 33	NA	17 ± 0.5	NA	14.7 ± 0.4
acetonitrile	19 / 42	48.2 ± 0.3	42.2 ± 0.3	38.6 ± 0.4	34.8 ± 0.3
acetaldehyde	19 / 45	42 ± 1	36 ± 1	32.7 ± 0.7	29.5 ± 0.5
acrolein	19 / 57	51.2 ± 0.8	44.6 ± 0.6	40.5 ± 0.5	38.8 ± 0.5
acetone	19 / 59	68.7 ± 0.8	57.7 ± 0.6	52.2 ± 0.6	47.0 ± 0.5
isoprene	19 / 69	27.2 ± 0.4	23.7 ± 0.3	18.7 ± 0.3	15.6 ± 0.2
2-butenal	19 / 71	76.3 ± 0.8	67.3 ± 0.5	61.6 ± 0.8	56.6 ± 0.4
butanone	19 / 73	71.7 ± 0.8	60.6 ± 0.5	56.1 ± 0.5	51.4 ± 0.3
benzene	19 / 79	43.3 ± 0.4	29.5 ± 0.3	20.9 ± 0.3	16.2 ± 0.2
toluene	19 / 93	29.6 ± 0.2	26.0 ± 0.2	23.0 ± 0.2	20.4 ± 0.2
o-xylene	19 / 107	56.6 ± 0.6	43.8 ± 0.4	33.1 ± 0.4	25.0 ± 0.3
a-pinene	19 / 137	30.3 ± 0.2	25.9 ± 0.2	22.3 ± 0.2	19.5 ± 0.2
dichlorobenzene	19 / 147	50.6 ± 0.3	31.5 ± 0.2	19.8 ± 0.2	12.2 ± 0.2
isoprene	30 / 68	13.5 ± 0.2	14.6 ± 0.3	15.6 ± 0.2	15.6 ± 0.2
2-butenal	30 / 69	46.2 ± 0.5	50.2 ± 0.3	53.5 ± 0.5	52.9 ± 0.4
benzene	30 / 78	27.8 ± 0.3	30.0 ± 0.3	30.0 ± 0.3	29.6 ± 0.3
toluene	30 / 92	73.6 ± 0.5	78.4 ± 0.6	78.4 ± 0.5	77.9 ± 0.4
butanone	30 / 102	4.7 ± 0.2	6.3 ± 0.2	7.6 ± 0.2	7.7 ± 0.1
***o*-xylene**	30 / 106	48.8 ± 0.4	52.5 ± 0.6	53.2 ± 0.4	52.4 ± 0.4
chlorobenzene	30 / 112	42.6 ± 0.4	46.4 ± 0.3	47.5 ± 0.4	47.0 ± 0.4
α-pinene	30 / 136	4.7 ± 0.1	5.9 ± 0.1	6.5 ± 0.2	5.7 ± 0.2
dichlorobenzene	30 / 146	27 ± 0.4	25.2 ± 0.3	24.1 ± 0.4	23.2 ± 0.3
2-butenal	32 / 69	5.3 ± 0.2	6.8 ± 0.2	6.9 ± 0.3	7.1 ± 0.2
butanone	32 / 72	23.4 ± 0.3	25.8 ± 0.3	26.4 ± 0.3	26.9 ± 0.2
benzene	32 / 78	37.1 ± 0.3	41.7 ± 0.3	43.2 ± 0.3	44.2 ± 0.3
toluene	32 / 92	21.9 ± 0.2	24.2 ± 0.2	25.1 ± 0.3	26.3 ± 0.2
α-pinene	32 / 93	32.7 ± 0.3	35.6 ± 0.2	38.3 ± 0.3	38.4 ± 0.3
chlorobenzene	32 / 112	28.2 ± 0.3	30.7 ± 0.3	33.0 ± 0.3	32.6 ± 0.4
dichlorobenzene	32 / 146	NA	17.0 ± 0.5	NA	14.7 ± 0.4

Table S10: SNR at 1 ppb, upper and lower confidence interval (based on product ion counts normalized to 10^6 reagent ion counts, p = 95%, df = 7) of the PTR-MS of the different compounds for the different humidities at 25°C. n.d.: intensities were not measured at this *m/z* and humidity. Inf: infinite value, I(Blank) = 0.

compound	m/z	dry			30% humidity			60% humidity			90% humidity		
		SNR	CI^u	CI^l	SNR	CI^u	CI^l	SNR	CI^u	CI^l	SNR	CI^u	CI^l
methanol	33	1.2	1.5	0.9	1.2	1.5	0.9	1	1.8	0.4	1.2	1.4	1
acetonitrile	42	130	2330	-10	190	830	-40	n. d.	n. d.	n. d.	n. d.	n. d.	n. d.
acetaldehyde	45	2.4	3.3	1.6	2.5	3.5	1.7	n. d.	n. d.	n. d.	n. d.	n. d.	n. d.
acrolein	57	16	81	2	33	138	6	n. d.	n. d.	n. d.	n. d.	n. d.	n. d.
acetone	59	49	526	2	39	176	8	31	60	15	67	265	16
isoprene	69	25	527	-6	28	122	3	54	1125	-6	22	918	-1
2-butenal	71	23	109	3	132	1377	6	165	647	-32	70	465	7
butanone	73	6.7	15.3	2.5	42	125	12	21	70	5	1	179	-1
benzene	79	34	156	6	76	1067	3	n. d.	n. d.	n. d.	n. d.	n. d.	n. d.
toluene	93	7.9	18.4	3.1	12	31	4	16	38	6	12	22	6
***o*-xylene**	107	14	28	6	14	43	4	n. d.	n. d.	n. d.	n. d.	n. d.	n. d.
α-pinene	137	80	220	-20	220	410	-60	80	670	-10	160	300	-50
dichloro-benzene	148	Inf	Inf	Inf	39	56	-20	n. d.	n. d.	n. d.	n. d.	n. d.	n. d.

5

Table S11: SNR at 1 ppb ± 95% confidence interval, based on product ion counts normalized to 10^6 reagent ion counts, df = 7) of the SIFT-MS of the different compounds and relative humidities at 25°C. NA: LOD was over 2 ppb so that not enough calibration points remained for a calibration.

compound	m/z_{reag} / m/z_{prod}	dry			30% humidity			60% humidity			90% humidity		
		SNR	CI^u	CI^l	SNR	CI^u	CI^l	SNR	CI^u	CI^l	SNR	CI^u	CI^l
methanol	19 / 33	1.1	1.6	0.8	1.3	1.8	0.9	1.3	2.3	0.5	1.4	2.3	0.7
acetonitrile	19 / 42	18	182	-1	21	1013	-1	15	46	4	10	30	2
acetaldehyde	19 / 45	1.2	1.5	0.9	1.2	1.5	0.9	1.2	1.6	0.9	1.3	1.7	0.9
acrolein	19 / 57	1.7	2.6	1.1	2.1	3.6	1	2.3	3.5	1.4	2.4	3.6	1.5
acetone	19 / 59	1.8	2.8	1.1	2.3	3.6	1.4	1.6	2.5	0.9	2.2	3.3	1.3
isoprene	19 / 69	3.6	8.4	1.2	4.6	12	1.3	2.8	5.5	1.1	3.5	9.2	0.7
2-butenal	19 / 71	2.1	4.5	0.5	4.6	7	2.8	2.5	4.7	0.9	2.8	4.1	1.8
butanone	19 / 73	3.3	4.8	2.1	4.3	7.4	2.2	3.2	5.4	1.6	4.1	6.8	2.2
benzene	19 / 79	13	34	4	15	56	2	9.4	31.8	1.9	11	38	2
toluene	19 / 93	30	145	5	22	162	1	9.8	28.2	1.9	9.7	25.9	2.3
***o*-xylene**	19 / 107	24	177	1.9	26	86	6	18	75	3	12	30.2	3.7
α-pinene	19 / 137	14	37	3	19	65	4	12	46	2	13	27.1	5.3
dichlorobenzene	19 / 147	33	188	2	34	225	0	21	1129	-3	11	53	0
isoprene	30 / 68	9.4	35.8	1.4	8.6	96.1	-0.7	11	116	-1	12	61	0
2-butenal	30 / 69	3.3	8.1	0.8	7.5	17.1	2.4	4.7	11.6	0.9	5.3	10.1	2.5
benzene	30 / 78	17	52	4	23	97	3	20	61	3	22	71	5
toluene	30 / 92	59	234	11	55	167	14	54	144	17	62	200	15
butanone	30 / 102	8.5	119.8	-1.3	6.4	63.1	-0.7	4.1	18.7	-0.2	6.8	62.1	-0.3
***o*-xylene**	30 / 106	27	278	2	42	156	6	29	173	3	25	93.7	5.6
chlorobenzene	30 / 112	6.1	10.2	3.1	6.4	12.9	2.8	6.7	13.4	2.7	6.5	11.7	3.1
α-pinene	30 / 136	10	48	-4	7.3	64.8	-1.4	5.5	35.8	-0.5	4.7	19.3	0.1
dichlorobenzene	30 / 146	37	952	-1	32	202	2	26	136	2	38	174	6
2-butenal	32 / 69	2.3	5.3	0.7	5.2	12.9	1.6	2.4	4.9	0.9	2.7	5.6	0.9
butanone	32 / 72	2.8	10.3	-0.2	3.3	8.8	0.6	2.1	6.6	0.3	2.7	5.6	0.9
benzene	32 / 78	12	43	3	12	34	3	9	22.7	3	12	35	3
toluene	32 / 92	28	165	4	40	350	2	31	472	-1	27	105	5
α-pinene	32 / 93	24	170	1	22	103	3	21	157	1	17	147	0
chlorobenzene	32 / 112	11	32	3	11	27	4	9.9	18.1	5	11	30	3
dichlorobenzene	32 / 146	43	259	-12	70	1233	-1	25	268	0	24	113	3

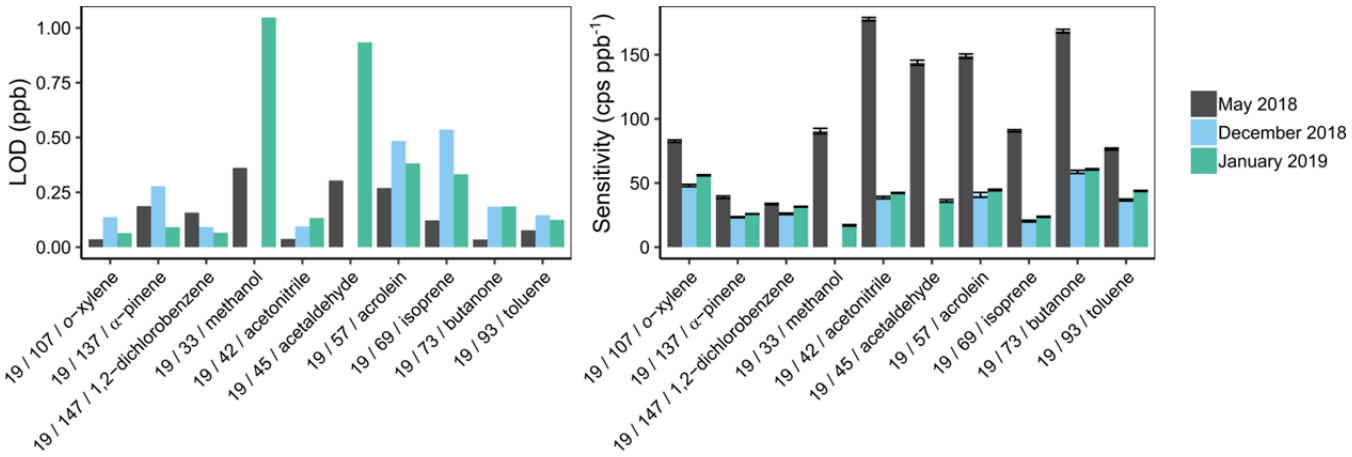

Figure S22: Robustness of calibrations of the SIFT-MS. The calibrations in May, December and January show considerable differences as one can see from the LOD changes (left panel) and sensitivity changes (right panel). This might be due to the o-ring change in September and a detector breakdown end-December. Both times, repairs were necessary. Still, a regular calibration should be done at least after each maintenance and if possible before every important experiment.

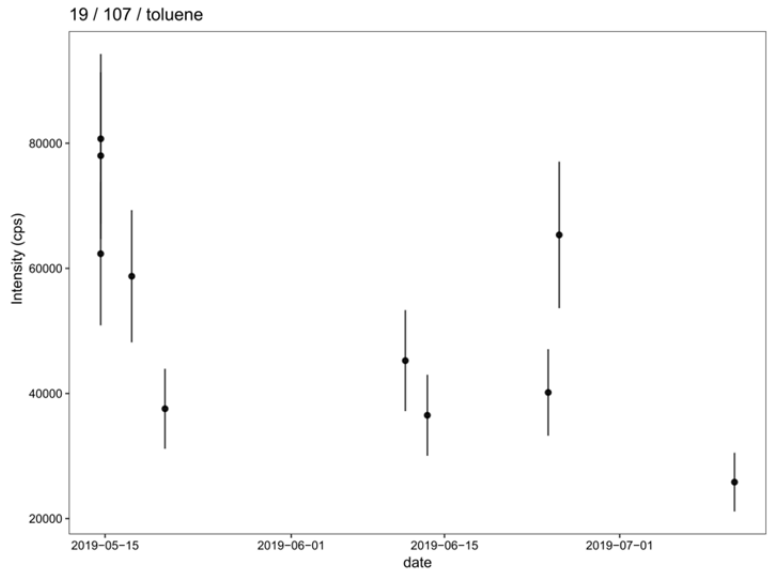

Figure S23: Long-term signal stability of the SIFT-MS tested with a standard of 2 ppm toluene. The Neumann trend test does not indicate a trend (p = 95%, n = 10).

References

Smith, D. and Spanel, P.: Selected ion flow tube mass spectrometry (SIFT-MS) for on-line trace gas analysis, Mass Spectrom. Rev., 24, 661-700, 2005, https://dx.doi.org/10.1002/mas.20033.